

Surface Rupture of the 2005 Kashmir, Pakistan, Earthquake and Its Active Tectonic Implications

by Heitaro Kaneda, Takashi Nakata, Hiroyuki Tsutsumi, Hisao Kondo, Nobuhiko Sugito, Yasuo Awata, Sardar S. Akhtar, Abdul Majid, Waliullah Khattak, Adnan A. Awan, Robert S. Yeats, Ahmad Hussain, Muhammad Ashraf, Steven G. Wesnousky, and Allah B. Kausar

Abstract To provide a detailed record of a relatively rare thrust surface rupture and examine its active tectonic implications, we have conducted field mapping of the surface rupture associated with the 2005 M_w 7.6 Kashmir earthquake. Despite the difficulty arising from massive earthquake-induced landslides along the surface rupture, we found that typical pressure ridges and warps extend northwestward for a distance of ~ 70 km, with a northeast-side-up vertical separation of up to ~ 7 m. Neither the main frontal thrust nor the main boundary thrust is responsible for the earthquake, but three active faults or fault segments within the Sub-Himalaya, collectively called the Balakot–Bagh fault, compose the causative fault. Although the fault exhibits substantial geomorphic expression of repeated similar surface ruptures, only a part of it had been mapped as active before the earthquake. The location of the hypocenter suggests that the rupture was initiated at a deep portion of the northern–central segment boundary and propagated bilaterally to eventually break all three segments. Our obtained surface rupture traces and the along-strike-slip distribution are both in good agreement with results of prompt analyses of satellite images, indicating that space geodesy can greatly aid in time-consuming field mapping of surface ruptures. Assuming that the extensive fill terrace in the meizoseismal area was abandoned during 10–30 ka, we tentatively estimate the earthquake recurrence interval and shortening rate on the Balakot–Bagh fault to be 1000–3300 yr and 1.4–4.1 mm/yr, respectively. These estimates indicate that the Balakot–Bagh fault is not a main player of Himalayan contraction accommodation. © Selected field photographs and ArcGIS files of the mapped surface rupture traces and measured vertical separations are available in the electronic edition of *BSSA*.


Online Material: Field photographs and ArcGIS files of surface rupture traces and vertical separations.

Introduction

Onland active faults have caused many large destructive earthquakes, producing surface ruptures that contributed to growth of tectonic geomorphic features. Detailed mapping of coseismic surface rupture not only provides basic information to understand the earthquake itself and to estimate its recurrence interval, but adds fundamental insights for interpretation of tectonic geomorphic features elsewhere. However, surface ruptures of thrust type are much less common than strike-slip or normal ones, with only several well-documented examples worldwide in the last century (e.g., Rubin, 1996). Nonetheless, many large cities in the world are situated close to active thrusts and are exposed to serious seismic hazards. More information on thrust surface ruptures

thus needs to be accumulated for a better understanding and more rigorous seismic hazard assessment of active thrust faults.

The 8 October 2005 M_w 7.6 Kashmir, Pakistan, earthquake struck the westernmost part of the Indian-Eurasian collision zone, providing a rare opportunity to study a fresh thrust surface rupture, but at a sacrifice of more than 80,000 fatalities (based on the U.S. Geological Survey [USGS] earthquake center web site). The epicenter was located in the mountainous area ~ 100 km northeast of Islamabad, and the damage was particularly concentrated in the Pakistani-controlled Jammu-Kashmir. Although no historical large earthquake along the frontal Himalaya is reported to

have produced primary surface rupture (e.g., Bilham, 2004), prompt analyses of satellite images after the 2005 earthquake suggested coseismic surface faulting for a distance of ~80 km (Avouac *et al.*, 2006; Fujiwara, Tobita, Sato, Ozawa, Une, Koarai, *et al.*, 2006; Pathier *et al.*, 2006). Field evidence of the extensive thrust surface rupture was also found (Baig, 2006; Tapponnier, King, and Bollinger, 2006; Tapponnier, King, Bollinger, and Grasso, 2006; Yeats *et al.*, 2006) despite inaccessibility to and confusion in the meizoseismal area. Most of the surface rupture follows the preexisting traces of several active faults or fault segments, collectively called the Balakot–Bagh fault, the main part of which had been mapped before the earthquake as the active Tanda fault based on aerial photograph interpretation (Nakata *et al.*, 1991). Here we present results of our detailed field mapping of the surface rupture associated with the 2005 Kashmir earthquake to examine its relationship to preexisting tectonic geomorphic features (e.g., Nakata *et al.*, 1991; Kumahara and Nakata, 2006), regional geology (e.g., Calkins *et al.*, 1975), and source models of the earthquake (e.g., Fujiwara, Tobita, Sato, Ozawa, Une, Koarai, *et al.*, 2006; Parsons *et al.*, 2006). Preliminary earthquake recurrence and contribution of this fault to Himalayan convergence are also discussed. We also intend to provide basic raw information for future studies, and thus present long descriptive texts and detailed surface rupture maps,  as well as selected field photographs and

ArcGIS files of surface rupture traces and measured coseismic fault slip in the electronic edition of *BSSA*.

Tectonic, Geologic, and Seismologic Setting

The Indian plate is colliding with the Eurasian plate at geologic and geodetic convergence rates of 30–50 mm/yr (Fig. 1, inset; DeMets *et al.*, 1990; 1994; Sella *et al.*, 2002; Bettinelli *et al.*, 2006). About 15–20 mm/yr of that relative plate motion is presently accommodated across the Himalaya (e.g., Bilham *et al.*, 1997; Banerjee and Bürgmann, 2002; Bettinelli *et al.*, 2006), mostly by the main frontal thrust (MFT) that marks the southern margin of the Himalayan range (e.g., Lavé and Avouac, 2000; Kumar *et al.*, 2001). In Pakistan to the west, the northwest-trending Himalaya arc abruptly changes its strike to east–west to form the Hazara arc. The Salt Range thrust (SRT), an equivalent to the MFT, marks the southern margin of the Hazara arc, reportedly absorbing at least 9–14 mm/yr of north–south shortening (Baker *et al.*, 1988). North of the MFT or SRT lies the Sub-Himalaya, which is mainly composed of folded and faulted Mesozoic and Tertiary sedimentary rocks and foredeep molasse sediments. The Sub-Himalaya is bounded on the north by the main boundary thrust (MBT), north of which are partially metamorphosed Precambrian to Mesozoic rocks of the Lesser Himalaya. The MBT is mostly inactive, although it

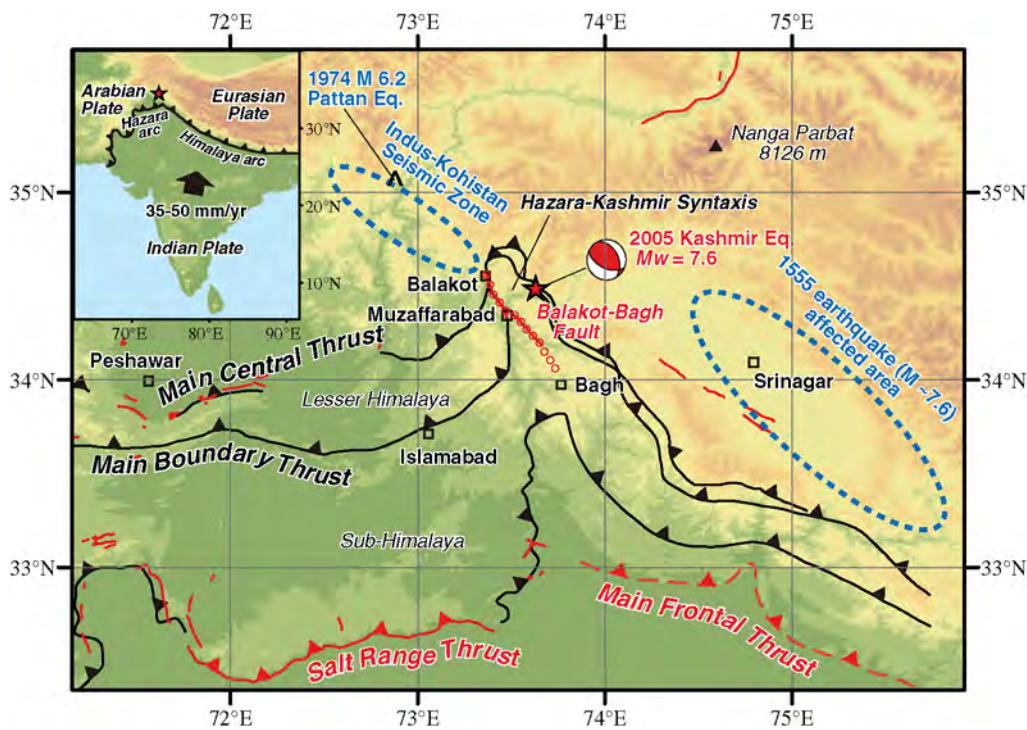


Figure 1. Regional tectonic map of the westernmost part of the frontal Himalaya. Solid black lines are major tectonic lines from Burg *et al.* (2005). Red lines show active faults from Nakata *et al.* (1991) and Avouac *et al.* (2006). The 2005 surface rupture is denoted by aligned red circles. Affected area of the 1555 earthquake (Ambraseys and Jackson, 2003) and the IKSZ (zone of high microseismicity; Armbruster *et al.*, 1978; Seeber and Armbruster, 1979) are also shown by blue dashed ellipses.

is known to locally displace late Quaternary surfaces and deposits in the Indian and Nepali Himalaya (e.g., Nakata, 1989). The 2005 earthquake occurred in a mountainous area ~200 km north of the SRT, but apparently close to where the MBT makes a hairpin turn (Fig. 1), forming the Hazara–Kashmir syntaxis.

A 16-km-long active fault had been previously mapped in this region in the course of mapping active faults of Pakistan based on interpretation of aerial photographs (Figs. 1 and 2; Nakata *et al.*, 1991). This northeast-dipping active thrust was named the Tanda fault, which cuts fluvial terrace

surfaces, providing clear evidence of late Quaternary faulting (Nakata *et al.*, 1991). After the 2005 earthquake, Kumahara and Nakata (2006) examined stereo-paired CORONA satellite images taken in 1971 and found that the geomorphologically expressed active Tanda fault further extends northwest and southeast with a total length of ~60 km, from Balakot to northwest of Chikar Khas (Fig. 2).

Faults had also been mapped along or close to the trace of the active Tanda fault and its extensions based on bedrock geology (Calkins *et al.*, 1975; Akhtar, Saeed, and Haussein, 2004; Akhtar,Waliullah, *et al.*, 2004; Anwar *et al.*, 2004;

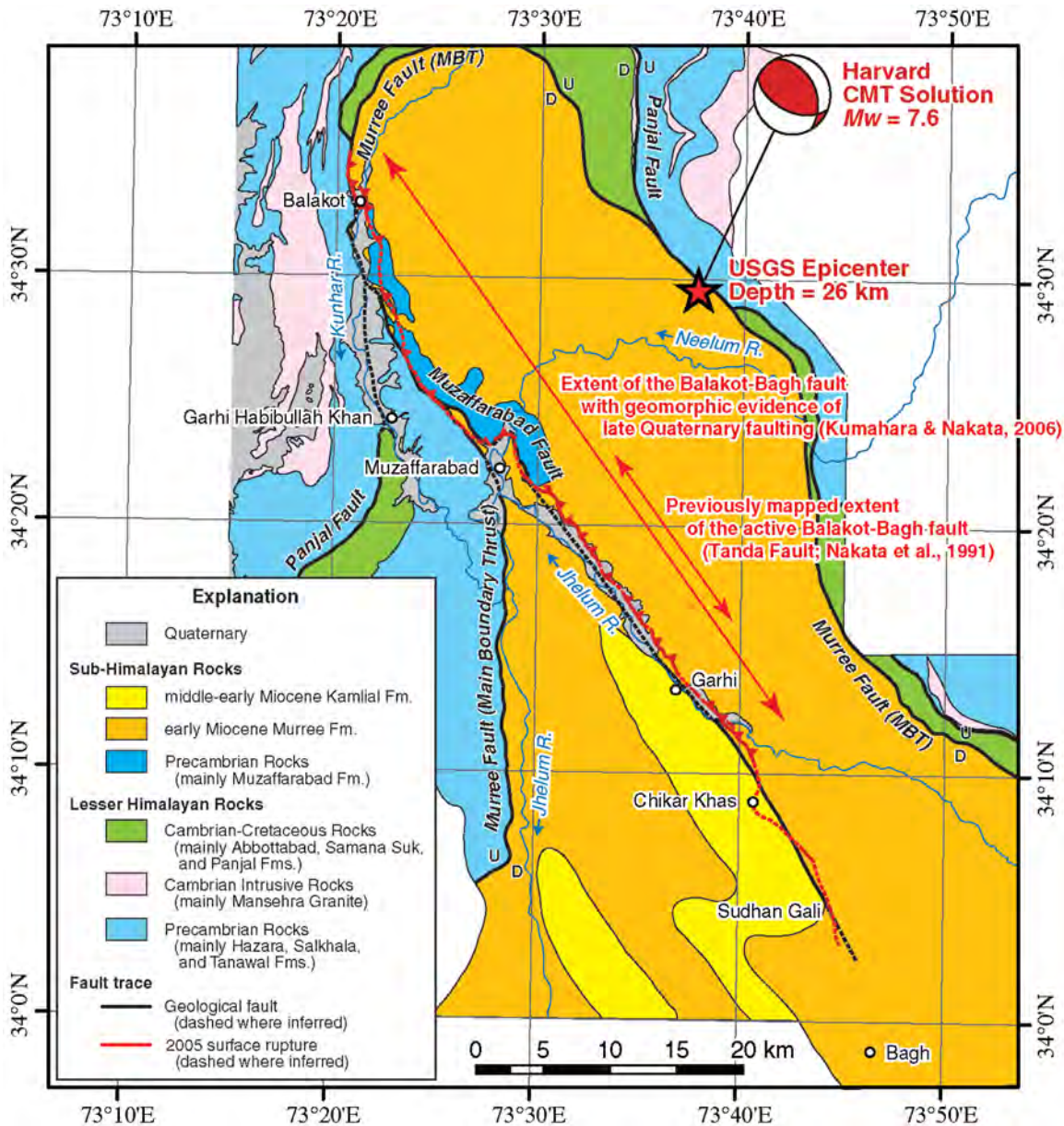


Figure 2. Geology in and around the epicentral area of the 2005 Kashmir earthquake. Compiled and simplified from the Geological Survey of Pakistan 1:50,000 geological map quadrangles (Akhtar, Saeed, and Haussein, 2004; Akhtar,Waliullah, *et al.*, 2004; Anwar *et al.*, 2004; Calkins *et al.*, 2004; Iqbal *et al.*, 2004) and the earlier 1:125,000 geological map (Calkins *et al.*, 1975). Trace of the 2005 surface rupture is also shown by red lines with teeth on the upthrown side.

Calkins *et al.*, 2004; Iqbal *et al.*, 2004). The northern part of the extended Tanda fault mostly runs along the northwest-trending Murree fault, a local name for the MBT, which separates the Sub-Himalayan rocks (Miocene molasse of the Murree formation and underlying Precambrian dolomite of the Muzaffarabad formation) on the northeast from the Precambrian Lesser-Himalayan rocks of the Hazara and Salkhala formations on the southwest (Fig. 2). Northwest of Muzaffarabad, the sinuous Muzaffarabad fault (Calkins *et al.*, 1975) bifurcates from the Murree fault to separate the Muzaffarabad formation to the northeast from the Murree formation to the southwest. Akhtar, Waliullah, *et al.* (2004), Anwar *et al.* (2004), and Iqbal *et al.* (2004) inferred that this fault extends southeastward to Sudhan Gali, northwest of Bagh. Although the extended part of the Muzaffarabad fault runs within Miocene Sub-Himalayan rocks, it partially divides the early Miocene Murree formation to the northeast from the slightly younger early-to-middle Miocene Kamliyal formation to the southwest. The active Tanda fault and its extensions appear to follow the trace of the Muzaffarabad fault, but no geomorphic evidence of late Quaternary faulting is recognized southeast of Chikar Khas along the extended part of the Muzaffarabad fault (Fig. 2; Kumahara and Nakata, 2006).

The 2005 earthquake struck one of the sections of the Himalaya where lack of a recent large earthquake had indicated potential for a great earthquake to release accumulated strain (Khattari, 1987; Bilham *et al.*, 2001). The most recent large ($M > 7$) earthquake known in and around the 2005 epicentral area is the 1555 Kashmir earthquake of $M \sim 7.6$, but the damage from the earthquake is reported to have been concentrated around Srinagar to the east (Fig. 1; Ambraseys and Jackson, 2003), suggesting that the 1555 and 2005 events were on different source faults. The 2005 meizoseismal area is also located just southeast of a northwest-trending belt of high microseismicity, called the Indus–Kohistan seismic zone (IKSZ) (Fig. 1; Armbruster *et al.*, 1978; Seeber and Armbruster, 1979). The 1974 M 6.2 Pattan earthquake occurred within the IKSZ (Pennington, 1979), claiming 5300 lives despite its moderate size. The 2005 aftershocks were also concentrated in this zone (Parsons *et al.*, 2006).

Response to the 2005 Earthquake

The epicenter determined by the United States Geological Survey (USGS) (34.493° N, 73.629° E; location uncertainty ± 3.6 km) is located northeast of the surface trace of the northeast-dipping active Tanda fault (Fig. 2). A fast moment-tensor solution by Harvard University suggests that the event is predominantly thrust type (strike is 333°, 116°; dip is 39°, 57°; slip is 121°, 68°; Figs. 1–3) with a seismic moment release of 2.9×10^{20} N m (equivalent to M_w 7.6), which was large enough to expect surface rupture along the Tanda fault. Distribution of damage and landslides, together with prompt analysis of Envisat synthetic aperture radar (SAR) images (Fujiwara, Tobita, Sato, Ozawa, Une,

Koarai, *et al.*, 2006; Pathier *et al.*, 2006) and advanced space-born thermal emission and reflection radiometer (ASTER) images (Avouac *et al.*, 2006), also suggested that the active Tanda fault or a series of geological faults (Murree and Muzaffarabad faults) were responsible for this earthquake. The Geological Survey of Pakistan collectively named those faults the Balakot–Bagh fault (e.g., Hussain and Yeats, 2006). Although the Balakot–Bagh fault is obviously subdivided into several faults or fault segments with different geological, geomorphological, and geometrical characteristics, we use this term to mean the causative fault of the 2005 earthquake for its familiarity in Pakistan.

Several lines of evidence suggested that the earthquake had produced surface ruptures along the Balakot–Bagh fault, but there was no robust field information about surface rupture from the epicentral area even a month after the earthquake. The first field evidence of surface faulting was provided at the Islamabad international conference in January 2006, by a Pakistani geologist, M. S. Baig (Baig, 2006). A French–Pakistani group (J.-R. Grasso and M. N. Mughal) had also found the surface rupture before the conference, a few pictures of which were shown at the conference by P. Tapponnier (Tapponnier, King, and Bollinger, 2006). Their results were later presented in detail at the Seismological Society of America annual meeting at San Francisco in April (Tapponnier, King, Bollinger, and Grasso, 2006). After the Islamabad conference, we made a one-week reconnaissance field survey (Yeats *et al.*, 2006) and confirmed that the distinctive surface rupture appeared just along the mapped trace of the active Balakot–Bagh fault. However, we found that some of the surface rupture had already begun to be modified or destroyed, requiring prompt execution of detailed mapping. We thus organized a Japanese–Pakistani collaborative team to map the 2005 surface rupture in detail. The mapping was intensively conducted on 8–19 March 2006, which was ~ 5 months after the earthquake.

Methods

In order to fully use our limited time, we simultaneously deployed two to three subteams, each working on a different part of the surface rupture. Places that were field checked are along and around the tectonic geomorphic features of the Balakot–Bagh fault, which are visible on enlarged ($\sim 1:20,000$) stereo-paired CORONA satellite images (mission 1115-1, taken on 15 September 1971) prepared by Y. Kumahara at Hiroshima University (presently at Gumma University). We also checked possible surface ruptures identified on web-available high-resolution postearthquake images of Quickbird (<http://earth.google.com/>, last accessed March 2006) and IKONOS (www.spaceimaging.com/, presently www.geoeye.com/, last accessed February 2008) satellites, and high-gradient areas in the SAR-derived surface deformation field provided by the Geographical Survey Institute, Japan (Fujiwara, Tobita, Sato, Ozawa, and Une, 2006; Fujiwara, Tobita, Sato, Ozawa, Une, Koarai, *et al.*, 2006).

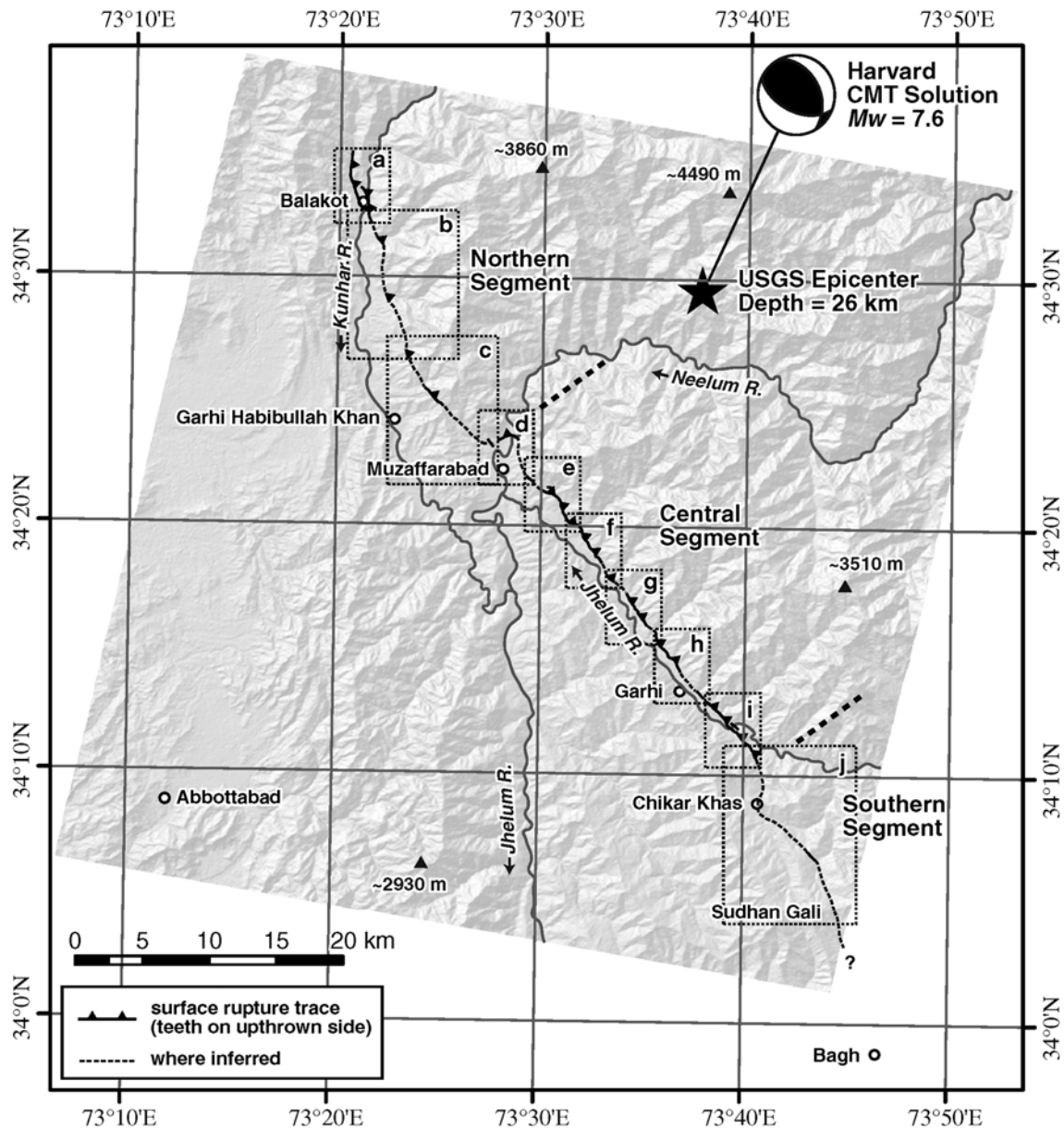


Figure 3. Geomorphology in and around the epicentral area of the 2005 Kashmir earthquake and the 2005 surface rupture trace. Dashed rectangles with labels indicate locations of detailed maps shown in Figure A1a–j. Background topographic relief image is based on the digital elevation model (DEM) produced by preearthquake ASTER images. Also shown are major peaks with approximate altitudes based on the DEM.

Although thorough mapping with no surface rupture missed is ideal, we were unable to check all the possible places because of logistic and security reasons. In particular, extensive earthquake-induced landslides along the northern part of the surface rupture (between Balakot and Muzaffarabad) prohibited the detailed mapping of this section of the fault. We thus need to acknowledge that some surface ruptures may be missed in our mapping, though we are sure that we covered most of the significant features.

Surface rupture was located using an ordinary portable Global Positioning System (GPS) receiver (Garmin eTrex series and similar models). The absolute horizontal accuracy

of the instrument is no better than 5–10 m but is good enough for our purpose of compiling the surface rupture at the scale of $\sim 1:25,000$. GPS readings were typically made every several tens of meters along the surface rupture.

Scarcity of artificial features with well-defined initial geometry across the fault trace prohibited slip-vector determination, which was successfully conducted for the 1971 San Fernando, California, earthquake (Sharp, 1975) and the 1999 Chi-Chi, Taiwan, earthquake (Lee *et al.*, 2003). We thus focus on determining only vertical separation due to surface faulting. Topographic profiles were taken across fault scarps and warps by using a portable electronic distance

meter with a precise tilt meter (Laser Technology Impulse 200; accuracy is ± 3 cm for a measured distance of 50 m). At some key sites, we also took profiles across composite scarps that resulted from multiple earthquakes, including the one in 2005. In order to formally measure vertical separation and estimate the associated uncertainty, we first visually divide the obtained profile into three sections: the upthrown side, deformation zone, and downthrown side (Fig. 4). Best-fit lines with $\pm 1\sigma$ uncertainty drawn from the upthrown and downthrown sides are used to determine maximum and minimum extremes, which are then converted to a preferred value \pm error. In most cases, the upthrown side was slightly steeper than the downthrown side, which may be due to broad tectonic tilt on the hanging wall. Alternatively, it may just represent nature of a fan surface that is usually steeper upstream. Given that profile length was typically 10–40 m, possible tectonic tilt broader than this is not included in our estimates. We also note that the determined vertical separation may be much less than apparent scarp height because back tilt or bulge on the crest of a scarp is included in the deformation zone (Fig. 4). By excluding such local features in measuring vertical separations, we can obtain measurements not biased by near-surface fault complexities, such as fault-dip variations, fault flattening, or fault branching. However, this tends to create a need for assigning a larger deformation zone and taking a longer profile, both of which lead to larger measurement uncertainty. Our assigned uncertainty includes all these effects.

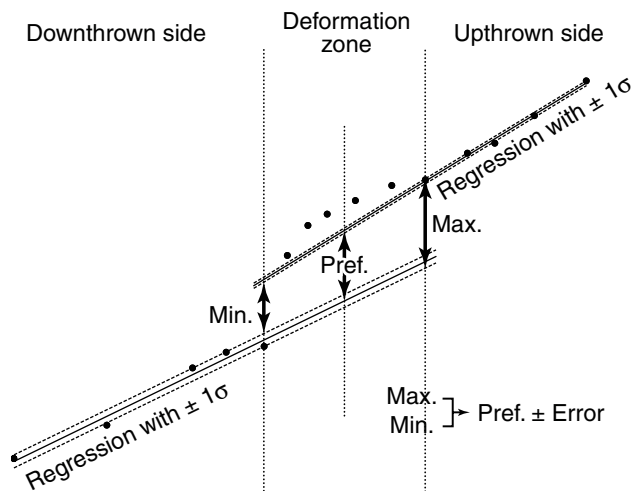


Figure 4. Formal assignment of vertical separation across the fault from an obtained topographic profile. Best-fit lines with $\pm 1\sigma$ uncertainty drawn from the upthrown and downthrown sides are used to determine maximum and minimum extremes, which are then converted to a preferred value \pm error. In most cases, the upthrown side was slightly steeper than the downthrown side, which is due to broad tectonic tilt on the hanging wall and/or is a representation of the nature of a fan surface that is usually steeper upstream. Given that profile length was typically 10–40 m, possible tectonic tilt broader than this is not included in our estimates.

General Features of the Surface Rupture

Precise traces and displacements of the 2005 surface rupture are revealed by 490 GPS-located points and 63 topographic profiles. The northwest-trending surface rupture extends for ~ 70 km from immediately north of Balakot to northwest of Bagh (Fig. 3). Typical surface expression of faulting is a northeast-side-up pressure ridge (e.g., Philip and Meghraoui, 1983; Philip *et al.*, 1992), that is, a monoclinical scarp with surface shortening features such as rolled-up or bulldozed turf at its base and extensive tension cracks on its crest. Bulging and back-tilting are also observed on the upthrown side at many places. At some places, the tension cracks formed on the scarp crest appear to exhibit a left-stepping en echelon pattern, implying a minor right-lateral strike-slip component. The amount of offset, however, could not be measured because of the lack of well-defined piercing points.

The surface rupture is subdivided into northern, central, and southern geometric segments separated by small steps (Fig. 3). The ~ 25 -km-long northern segment extends from north of Balakot to north of Muzaffarabad. The rupture exhibits northward bifurcation near its northern end, where geomorphic evidence also suggests fault branching (Kumahara and Nakata, 2006). To the southeast, the surface rupture passes through mountainous terrain, where extensive earthquake-induced landslides obscured or masked most of the surface rupture. Nonetheless, the highest fault scarp along the entire surface rupture was found on this mountainous section, a measured vertical separation being 7.05 ± 0.35 m. Although some sections of the surface rupture lie obviously east of surface trace of the MBT, the others appear to coincide with it (Fig. 2). However, slip sense is opposite: it is down to the southwest for the 2005 rupture, whereas it is down to the northeast for the geologically mapped MBT (e.g., Calkins *et al.*, 1975).

North of Muzaffarabad, the rupture makes an abrupt turn to trend almost east–west, producing an ~ 3 -km-long short lateral ramp connecting the northern and central segments. The maximum vertical separation on this lateral ramp is 2.45 ± 0.25 m. Unlike surface ruptures elsewhere, this short section is associated with a minor left-lateral component (~ 0.6 m), which is consistent with what is expected on a lateral ramp connecting left-stepping thrust segments. This east–west-trending surface rupture coincides both with the base of the preexisting fault scarps (Kumahara and Nakata, 2006) and the geologically mapped Muzaffarabad fault (Calkins *et al.*, 1975).

The central segment between Muzaffarabad and northwest of Chikar Khas is characterized by an almost continuously traced surface rupture that follows the surface trace of the active Balakot–Bagh fault. The surface rupture crosses numerous terrace surfaces and incised valleys for a distance of ~ 30 km, forming southwest-facing monoclinical scarps along the base of the preexisting fault scarps of various heights and ages. The maximum vertical separation mea-

sured on this segment is 4.6 ± 1.1 m. The rupture also extends close to and subparallel to the southeastward extension of the geological Muzaffarabad fault (Fig. 2; Akhtar, Waliullah, *et al.*, 2004; Iqbal *et al.*, 2004), implying that they coincide at least partially.

The southern segment between Chikar Khas and Bagh is a discontinuous surface rupture with relatively small displacement passing through mountainous terrain. We found tectonic features such as continuous mole tracks and cracks at only three localities on this segment, the southeasternmost being at Sudhan Gali, ~ 10 km northwest of Bagh. Although we were unable to make a reliable estimate, vertical separation is up to 1 m on this segment. The southern segment also extends close to the southeastward extension of the Muzaffarabad fault (Akhtar, Waliullah, *et al.*, 2004) but mostly does not coincide (Fig. 2).

Detailed Description of the Surface Rupture

Field-mapped surface rupture traces are compiled and shown in the maps in Figure A1. We here describe the surface rupture associated with the 2005 Kashmir earthquake from north to south, together with some field photographs (Figs. 5–10). \textcircled{E} Additionally, ~ 100 field photographs, which will aid in understanding the descriptions, are available in the electronic edition of *BSSA*. For descriptive purposes, we number the GPS-located points from the northern (location 001) to southern ends (location 490) along the surface rupture. \textcircled{E} Coordinates and other detailed information of the GPS-located points and measured vertical separations can be obtained by opening *GPS_point.dbf* and *Vert_Sep.dbf* files, available in the electronic edition of *BSSA*, with a spreadsheet software such as Microsoft Excel.

Geomorphic evidence for previous events is also noted where available. In particular, the Jhelum River, upstream of Muzaffarabad (upper Jhelum River), is characterized by an extensive fill terrace surface standing several tens of meters above the modern riverbed, providing excellent geomorphic markers to identify evidence for previous surface-rupturing events. We here tentatively term this key terrace surface the M surface in the descriptions. Another less extensively distributed terrace surface a few tens of meters above the M surface is called the H surface.

In and around Balakot (Fig. A1a, Locations 001–057)

The northern end of the mapped surface rupture is located ~ 3 km north of Balakot (location 001; see section Note Added in Proof at the end of the article for the extension further to the north), on a locally preserved terrace surface between Jalora Katha and Barna Katha (“katha” means a small stream in the local language). On the CORONA satellite images, a west-facing ~ 20 -m-high fault scarp is recognized on this surface (Kumahara and Nakata, 2006). The surface rupture appeared along the base of this cumula-

tive scarp (locations 001–007), forming west-facing fault scarps or warps up to ~ 1.6 -m high (location 003). A small dammed-up pond is also formed on the downthrown side (location 004). However, where the preexisting fault scarp is most clearly recognized (locations 005–006), the surface expression of faulting becomes indistinct, probably because of extensive scarp slope failures. At location 006, the rupture apparently meets a near vertical bedrock fault exposure between the Miocene Murree Formation to the east and the Precambrian Hazara Formation to the west, suggesting that the surface rupture coincides with the surface trace of the MBT here. The surface rupture is traced along the geologic boundary down to location 007, but soon becomes indistinct to the south. From location 001 to the north, the rupture may extend for a short distance along the western bank of Jalora Katha, but it could not be traced because of extensive slope failures (see section Note Added in Proof at the end of the article).

There is a 600-m-long gap in the surface rupture between locations 007 and 008, primarily due to extensive landslides. The rupture reappears on the left bank of Barna Katha along the western margin of the hills to the east. Well-defined, west-facing monoclinical scarps, up to ~ 1.95 -m high, are formed across paddy fields. The rupture traverses numerous paddy dikes, but with no systematic lateral offsets. South of location 016, it was impossible to trace well-defined surface rupture down to Balakot, although we found severely sheared bedrock exposed on streambed immediately north of Balakot Hill.

Extensive structural damage and loss of human lives occurred in downtown Balakot. Devastation is exclusively concentrated on the hanging-wall side of the thrust surface rupture (Fig. 5a), in particular on Balakot Hill (Old Balakot), where almost all the houses and buildings completely collapsed (Fig. 5b,c). According to local people, 1661 lives were lost on this small hill, which corresponds to 85% of the population living there. Balakot Hill is composed of basement rock overlain by round boulders, indicating that the hill is a remnant of a fluvial terrace surface. The hill shape is extremely asymmetric, with a moderate southwestern slope (20° – 30°) and steeply eroded northeastern and eastern flanks. The southwestern slope appears to be a tectonically tilted or warped terrace surface, the causative fault presumably running along the western margin of the hill. Our mapping confirmed that the surface rupture appeared from the western margin of Balakot Hill (location 029) southwestward to the Balakot Bridge (location 039). Between locations 029 and 035, monoclinical scarps can be traced continuously across vegetable fields that were flat prior to the earthquake. The vertical separation is ~ 0.45 m, but this value should be considered to be the minimum because we could not determine the amount of coseismic warping/tilting of the hill slope.

South of Balakot Hill, an alluvial terrace of probable Holocene age on which downtown Balakot has been developed is also warped into a broad west-facing monocline. The width of the deformation zone is about 20 m, and the vertical separation reaches about 2.65 m. Tension cracks develop ex-



Figure 5. (a) Oblique aerial photograph of Balakot taken one week after the earthquake during the United States helicopter relief mission. View west. The surface rupture trace is shown by a dashed red line, with red arrows indicating selected numbered localities. Note that structural damage is concentrated on the hanging-wall side (bottom side) of the thrust surface rupture. Photograph is courtesy of Wiley Thompson. (b) and (c) Balakot Hill (Old Balakot) before (b) and after (c) the earthquake. Looking northeast. Balakot Hill is interpreted as a tilted or warped remnant of a fluvial terrace surface, a causative fault presumably running along the southwestern margin of the hill (indicated by red arrows). The 2005 surface rupture appeared along this active fault trace, leaving incredible devastation on the hill. The preearthquake photograph is on the courtesy of Aamir Rashid. (d) Westward tilting of the base of the destroyed yellow-painted house (location 038) just southeast of Balakot Hill. The vertical separation is measured to be ~ 2.65 m here. Note that a tree on the background is also tilted. (e) Westward tilting is most clearly demonstrated by a small fountain basin at a school southeast of location 038. Looking northwest. The yellow-painted house and Balakot Hill are visible on the background.

tensively at the crest of the monocline. This monoclinical warping is especially well demonstrated by the westward tilting of the base of the yellow-painted house and a nearby fountain basin at location 038 (Fig. 5d,e). The main road along the Kunhar River is also vertically displaced immediately north of a small bridge (location 039) by ~2.5 m.

The surface rupture extends to the other side of the Kunhar River (locations 040–046). Where the rupture traverses the Kunhar River, an ~1-m-high waterfall has been developed on the river channel that was first identified on the IKONOS images (H. Une and Y. Kumaki, personal comm., 2005; Fig. 5a). Even 5 months after the earthquake, the waterfall is clearly identified although it has migrated upstream about 10 m. On the left bank of the Kunhar River, the rupture extends southeast for ~30 m and makes a sharp turn to northeast at location 41. The south-facing monocline between locations 041 and 046 is up to 1.45-m high. Although the sharp turn in the fault trace may cause substantial lateral slip between locations 041 and 046, the fault scarp is associated with no recognizable lateral slip component. From location 045, the amount of vertical offset decreases rapidly to the east and the rupture terminates where it intersects with a north-trending erosional scarp in the village of Garlot.

Another surface rupture strand is identified north of Balakot. About 800 m north of Balakot Hill, a northwest-trending surface rupture appeared for a distance of ~400 m south of Jalora (locations 017–028). Three preexisting northwest-trending linear scarps are identified on the CORONA satellite images in and around Jalora (Kumahara and Nakata, 2006), but field observations confirmed that the surface rupture appeared only along the northernmost lineament. The rupture appeared at the base of gentle, degraded monoclinical scarps several meters high, suggesting that similar deformation has taken place repeatedly in the past. We could not trace the surface rupture north of location 017 due to extensive landslides, but the fault along which the surface rupture appeared traverses the hill between the Kunhar River and Barna Katha to merge with the surface rupture along Barna Katha (locations 008–016).

No surface deformation was identified southeastward from location 028 to the Kunhar River. However, further south, at locations 047 and 048, we found a warped small alluvial fan and buckled asphalt road, respectively, which probably reflect tectonic deformation. Southward from location 049, well-defined monoclinical or fault scarps intermittently appeared for a distance of ~500 m along the fault that separates fluvial terraces of the Kunhar River from the mountain ranges to the east. The vertical separation is up to 1.7 m. Immediately south of location 057, we were not able to identify coseismic deformation along Bheran Katha.

Balakot to Muzaffarabad (Fig. A1b,c,
Locations 058–114)

The surface rupture between the Kunhar River south of Balakot and the Neelum River north of Muzaffarabad passes

through mountainous terrain where rugged topography and earthquake-induced landslides did not allow us to continuously trace the rupture. We instead checked major tributaries of the Kunhar River, which should cross the fault.

A spectacular fold scarp appeared across the riverbed of Khwas Katha (location 067) about 1.8 km southeast of location 057. The scarp produces a distinctive waterfall, with a vertical separation reaching ~5.7 m. On the left bank of the Khwas Katha, strata are widely exposed due to slope failure. The surface rupture coincides with a fault juxtaposing dolomite of the Muzaffarabad Formation to the east and sandstone/shale of the Murree Formation to the west. Presence of the Miocene Murree Formation west of the rupture indicates that the surface rupture here does not coincide with the surface trace of the MBT. North of Khwas Katha, smaller surface rupture appeared along the northwest-trending topographic boundary between the bedrock ridge and fluvial terrace (locations 058–065).

To the south, we checked in and around the village of Naukot that is located on a high flatland probably produced by an ancient landslide. However, we were unable to find distinctive fault rupture, except for a short northwest-trending thrust with a 10- to 20-cm vertical separation that could result either from tectonic or gravitational forcing. We also walked down to Laranji Katha just south of Naukot, but the valley floor is almost completely filled by landslide deposits shed from both sides of the valley, masking possible surface rupture. Two powerline towers are significantly tilted at the outlet of Laranji Katha. Those deformations, however, appear to be gravitational although we found heavily sheared bedrock nearby.

A clear fault scarp reappears across Shishar Katha, where the riverbed is warped into a monocline, forming a waterfall that had been significantly degraded by the time of our visit in March 2006 (location 080; Fig. 6a). Topographic profiling along the right bank of the stream reveals a vertical separation of 7.05 ± 0.35 m (Fig. 6b), the maximum value recorded along the entire surface rupture of the 2005 earthquake. The surface rupture can be traced northward onto a low fluvial terrace on the right bank of Shishar Katha. A typical fold scarp, up to 2-m high, with a bulge on the upthrown side appears at the base of a preexisting ~5-m-high fault/fold scarp that is visible on the CORONA satellite images.

Sarwai Katha is another stream ~3.9 km south of Shishar Katha. On the left bank of Sarwai Katha, a narrow fluvial terrace more than 50 m above the present channel forms a west-facing fault scarp (Kumahara and Nakata, 2006) ~20-m high based on a handheld GPS. Surface rupture appeared at the base of the scarp for a distance of 100 m (locations 085–089). The west-facing monoclinical scarp with a bulge exhibits a maximum displacement of 0.85 m in 2005. We could not identify clear surface rupture across Sarwai Katha by observing from the top of the terrace.

Along Sorida Kashkar (also called Hassari Katha), a major tributary ~3 km south of Sarwai Katha, we were not

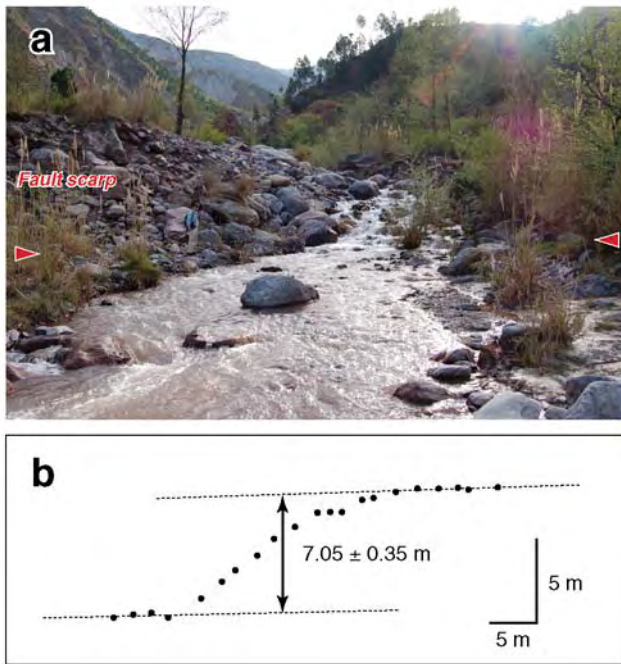


Figure 6. (a) Fault scarp across Shishar Katha at location 080 (a huge scarp immediately behind the person). Base of the scarp is indicated by red arrows. The scarp traverses a stream forming a waterfall, which has been significantly degraded. (b) Topographic profile across the scarp. The vertical separation of ~ 7.05 m was the largest measured along the entire surface rupture.

able to identify clear evidence for coseismic deformation. The fault probably passes where landslide deposits from both sides of the valley filled the valley floor.

We walked the 2-km-long stretch from the Sorida Kashkar southeastward to Dub Gali, along a topographic break indicative of a geologic boundary. Although numerous landslides along the fault made it difficult to trace the surface rupture continuously, we were able to identify coseismic ruptures at several localities. Tectonic warping is visible from locations 090 to 095. A paddy field is warped down to the west with a vertical separation of 2.15 m northwest of location 095. A north-trending, west-facing monocline identified between locations 096 and 098 could be related to a landslide because the site is located within a landslide block. A spectacular monoclinical scarp appeared across rice fields in the valley bottom of a tributary of the Sorida Kashkar (locations 099–105). The scarp is as high as ~ 3.0 m with a tectonic bulge ~ 0.6 m in height, the total vertical separation being 2.4 m. Pronounced back-thrusts are also present, indicating a large amount of crustal shortening. South of location 105, the surface rupture appears to extend along the break of slope angle, but its exact location is hard to locate due to extensive slope failure. Between locations 106 and 107, a short monoclinical scarp appeared in a paddy field. The vertical separation is only about 50 cm; this is probably part of a larger coseismic deformation. A west-facing monoclinical scarp with a vertical separation of ~ 1.9 m ap-

pears at a ridge from locations 108 to 111. At locations 112 to 114, a ~ 50 -cm-high, southwest-facing scarp appeared for a distance of 100 m. At Dub Gali, we were not able to identify any deformational features except for numerous landslides. We did not conduct detailed mapping along the section southeast of Dub Gali because of extensive landslides and lack of geomorphic features indicative of recent repeated surface faulting.

Around Muzaffarabad (Fig. A1d, Locations 115–149)

Surface rupture north of Muzaffarabad is characterized by anomalously trending fault/fold scarps. At Shawai Katha, a tributary of the Neelum River, we found a spectacular east–west-trending fault scarp that traverses the valley floor (locations 115–118). The present riverbed and a slightly higher grassy surface on the left bank are warped together, forming an ~ 2.45 -m-high monoclinical scarp. The waterfall produced by faulting was considerably degraded at the time of our visit. The fault scarp makes an abrupt turn at location 115 to trend northwest and appears to continue upstream along the valley. The local landowner, however, did not allow us to trace it further upstream. To the east, the scarp is completely covered by landslide deposits immediately east of location 118.

We checked on a double-crested ridge east of Shawai Katha, but no east–west-trending rupture was recognized. We instead found a curious northwest-trending rupture along the ridge trough (locations 119–124). The rupture is an ~ 600 -m-long southwest-facing scarp with up to ~ 2 m of vertical separation. The northern part of the rupture is a monoclinical scarp indicative of horizontal shortening whereas the southern part is a nearly vertical scarp with a scarp free face exposed. We did not recognize features indicative of significant extension such as open cracks along the rupture. From the scarp morphology, trace, and slip vector, we interpret that the rupture here is unlikely to be a gravitational feature, but probably tectonic in origin, at least in part, despite its location on a ridge top.

An east–west-striking surface rupture reappears north of Chehla Bandi for a distance of ~ 1 km (locations 126–145). The rupture follows the base of a preexisting fault scarp/warp (Kumahara and Nakata, 2006) that marks the southern margin of several fluvial terraces with increasing height to the west (Fig. 7a). Those surfaces appear to be warped southward and slightly back tilted northward with larger deformation for higher surfaces.

After buckling floors of several houses at locations 126–128, the fault becomes distinct from location 129. The south-facing fault scarp is almost continuously traced eastward with up to 2.15 m of vertical separation. At location 134, the scarp crosses a main road that leads to the upper Neelum, forming a few-meters-high gentle drop.

The surface rupture climbs down the north–south-trending ~ 10 -m-high terrace riser just east of the road to exhibit impressive features from location 136 to the east. A



Figure 7. (a) Distant view of deformed fluvial terrace surfaces at Chehla Bandi, north of Muzaffarabad. View northwest. A flight of several terrace surfaces with increasing height to the west (T1–T5) are all abruptly truncated by an east–west-trending fault indicated by red arrows. Back-tilt is also evident, in particular for upper surfaces (T1–T2). The 2005 surface rupture faithfully follows the base of the pre-existing fault scarps. Selected numbered localities on the surface rupture are also shown. (b) The 2005 surface rupture immediately in front of the preexisting fault scarp (location 137). Looking east. Bulging is well demonstrated by a concrete slab and regularly aligned fence posts indicated by vertical red arrows. (c) Two neighboring posts, which were ~3.3 m apart before the earthquake, are now standing very close, indicating a considerable amount of horizontal shortening. Tape measurement of each post interval yields horizontal shortening of ~4.6 m. Although not visible in the photograph, the aligned posts also show minor left-lateral offset of ~0.6 m here (© see Photo d-13 of the electronic edition of BSSA).

continuous fold scarp appears along the base of the east–west-trending ~20-m-high fault scarp, on which severe structural damage occurred. At locations 136–137, a turf surface was thrust onto a graveled surface, forming a 2.2-m-high monoclinal scarp ~20 m in front of the base of the preexisting scarp. A concrete slab east of location 137 also shows spectacular bulging (Fig. 7b). A row of fence posts just east of the concrete slab, which is nearly perpendicular to the surface rupture trace, serves as an excellent marker to measure horizontal shortening as well as strike-slip offset. Post intervals well away from the deformation zone are quite regular around 3.3 m, but two neighboring posts are now standing very close at the base of the fold scarp (Fig. 7c), indicating

considerable amount of horizontal shortening. Distances of other neighboring posts also appear to be somewhat shortened within the deformation zone with the exception of ~10 cm extension across the bulge crest. Tape measurement of each post interval suggests horizontal shortening of ~4.6 m here, assuming a regular post interval of 3.3 m prior to the earthquake. A minor left-lateral component of ~0.6 m is also evident from offset of linearly aligned fence posts. Just west of this site, a small trench was excavated across the 2005 surface rupture, exposing a fault dipping ~20° north (H. Kondo *et al.*, unpublished manuscript, 2007).

To the west, the fault scarp soon merges with the base of the preexisting fault scarp and becomes masked by extensive

slope failures. Small fold scarps with a height of up to a few tens of centimeters have developed in front of the preexisting scarp, but those features probably reflect only a part of the deformation. The height of the preexisting fault scarp decreases as we approach to the Neelum River, and finally becomes ~5 m east of location 145. Initially, this scarp was thought to be entirely due to the 2005 event, based on conversation with locals (Yeats *et al.*, 2006), but a soldier of the Nisar Camp located on the upthrown side of the scarp said that there already had been a small scarp or slope, and it grew during the earthquake.

The fault scarp is abruptly truncated at location 145 by a dry riverbed, on which no deformation is recognized (Fig. 7a). This was the ephemeral riverbed of the relocated Neelum River due to huge earthquake-induced failures of a dolomite slope to the east. According to the soldiers, the landslide debris was excavated by three missile shots three days after the earthquake to make a current river course to the east. We also found on the other (eastern) side exposure of the present Neelum that fluvial sands and gravels are beautifully warped into a monocline by several meters. Location of this monoclinical deformation suggests that the fault makes a gentle southeastward bend east of location 145.

Because of extensive landslides, we did not conduct detailed mapping from Chehla Bandi to Maira Tonoulian, southeast of Muzaffarabad. We only checked along the accessible roads, finding no rupture of possible tectonic origin. There is no geomorphic evidence of repeated active faulting along this section, but the landslides are exclusively concentrated along north-south-trending slope breaks that correspond to geologic boundary of Precambrian dolomite Muzaffarabad Formation to the east and Miocene sandstone/siltstone Murree Formation to the west. At Maira Tonoulian, we found an ~200-m-long northwest-trending fault scarp along the base of the steep mountain slope (locations 146–149). The scarp is severely modified by extensive scarp slope failures, but the vertical separation appears to be a few meters. At location 149, the scarp abruptly disappears beneath landslide debris.

Khella to North of Sehli Katha (Fig. A1e, Locations 150–187)

The northwest-flowing upper Jhelum River is characterized by well-developed fluvial terraces on the right bank, including the H and M surfaces (defined earlier in this article). Those fluvial surfaces are cut by a northwest-trending and northeast-dipping active thrust, forming southwest-facing cumulative fault scarps or warps of various heights (Nakata *et al.*, 1991; Kumahara and Nakata, 2006). The surface rupture is almost continuously traced along the trace of this active thrust.

At Khella, ~1.2 km southeast of Maira Tonoulian, severe house damage was concentrated along the base of preexisting fold scarps formed on terrace surfaces, which appear to be correlated to the H surface (locations 150–151).

Although no distinctive surface rupture is recognized, local people told that large horizontal shortening of up to ~6 m occurred during the earthquake, narrowing backyards of those houses. In the stream to the east, we found a bent and buckled road-side culvert at location 155, implying that some tectonic shortening occurred here.

Spectacular ~300-m-long uphill facing scarps develop on a mountain slope above the village of Khella (locations 152–154). The scarps are typically 1–2-m high, predominantly extensional, and follow preexisting similar features that are visible on the CORONA satellite images. Although the scarps could be explained by toppling type mass movement, they are not located on or close to a ridge crest, but in the middle of a mountain slope. We thus suspect that they could be related to tectonic extension developed on the upthrown side of the thrust.

The main surface rupture becomes evident at Tanda (locations 156–159), where a small wheat field is warped and back-tilted with a net vertical separation of 0.85 m. The rupture dies out after passing through a saddle at Tanda (location 159), but reappears to the southeast on wheat fields at locations 160–161 and a streambed at location 162. Surface profiling of the spectacular fault scarp that crosses the sandy streambed yields a vertical separation reaching ~4.6 m.

Surface expression of faulting is less distinct on the H terrace surface on which the village of Mang Umar Khan and the Muzaffarabad Airport are located. The H surface is vertically displaced by 50–60 m due to repeated surface faulting (Kumahara and Nakata, 2006), but relatively small (~1-m-high) discontinuous fold scarps/shortening features and severe house damages were found along the base of the preexisting scarp (locations 163–168).

An 18-yr-old man in this village witnessed the moment of surface faulting. Manshad Nakvi was sitting down and chopping wood at the time of the earthquake. He described that he heard a sound like a bomb blast, and a second later the ground started trembling. Severe shaking came a few seconds after he heard the sound. After another second, the ground moved very quickly to form a small scarp in front of him. He then fell down into an open crack that had formed beneath him.

At location 169, the fault crosses a small stream, forming an ~2.05-m-high monoclinical scarp. The rupture then makes an abrupt turn to trend north-south. The fault scarp continues downstream on the left bank for a distance of ~100 m and then up onto a low terrace surface at location 172. On the terrace, paddy fields appear to be slightly warped by a few tens of centimeters, but the surface rupture becomes a series of cracks south of location 173. The rupture again changes its direction to northwest at location 174. An obscure warp between locations 174 and 175 dies out southeast of location 175. Although the surface rupture appears to extend through a small saddle at location 177 farther southeastward, extensive landslides did not allow us to recognize distinctive tectonic deformation for a distance of ~700 m.

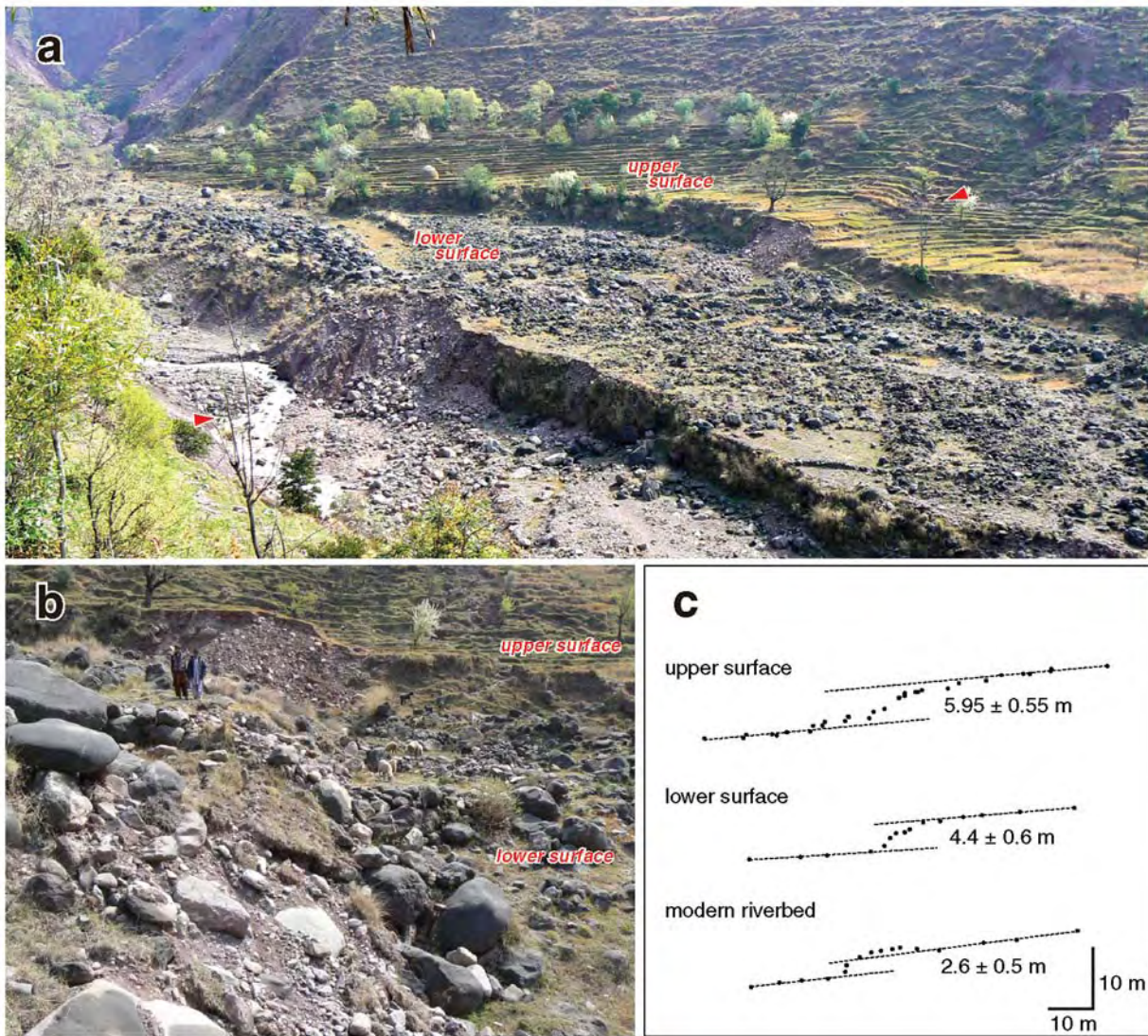


Figure 8. (a) Surface rupture across valley floor of Sehli Katha (locations 188–192). Looking east. A flight of two low terrace surfaces (lower and upper surfaces) of probable Holocene age are deformed in addition to the modern riverbed. Note that a paddy field on the upper terrace surface is narrowly divided on and around the fault trace, suggesting a preexisting fault warp on this surface. Quickbird high-resolution satellite images of this locality before and after the earthquake are shown in figure 3c of Pathier *et al.* (2006). (b) Monoclinical fault scarp on the lower surface extending onto the upper surface on the background. Looking southeast. Note that the terrace riser failed where it crosses the fault. (c) Topographic profiles of the upper, lower, and modern riverbed surfaces. Progressively increasing vertical separation for higher surfaces may indicate progressive number of earthquakes recorded on those surfaces. However, we cannot rule out the possibility that the lower surface scarp resulted only from the 2005 event, reflecting variable slip along the fault trace.

The surface rupture reappears at location 179, just north of Bagh Kardala, where we found a buckled paved road. Surface expression of faulting becomes even more distinct between Locats. 180 and 182. A southwest-facing monoclinical scarp, up to ~ 1.1 -m high, is continuously recognized along the topographic boundary between mountains and the H terrace surface. Just north of Sehli Katha, the surface rupture steps to the east and appears along the base of a preexisting fault scarp on the H terrace surface (locations 183–187). Paddy fields are warped into a monocline for a distance of ~ 300 m, but the vertical separations are relatively small (up to 0.8 m).

Sehli Katha to Prak da Katha (Fig. A1f, Locations 188–271)

A spectacular fault scarp crosses the valley bottom of Sehli Katha (locations 188–192) on which a flight of two low terrace surfaces of probable Holocene age occur (Fig. 8a). The location of the surface rupture at the valley bottom relative to those on the H surface indicates that the fault is a northeast-dipping low-angle thrust. The present riverbed exhibits monoclinical deformation with distinctive back-tilting, a net vertical separation being 2.6 ± 0.5 m (location 188; Fig. 8b). The topographic profiling of the lower and upper terrace surfaces yields vertical separations of 4.4 ± 0.6 m

and 5.95 ± 0.55 m, respectively. Progressively increasing vertical separation for higher surfaces may indicate progressive numbers of earthquakes recorded on those surfaces; that is, two seismic events were recorded on the lower surface, and three seismic events were recorded on the upper surface. At least the upper surface scarp results from multiple events because a paddy field on this surface is narrowly divided on and around the fault trace, suggesting a preexisting fault warp on this surface. However, we cannot rule out the possibility that the lower surface scarp is from a single earthquake, reflecting variable slip along the fault trace.

The fault appears on a distinctive ridge saddle to the south, forming a clear flexure scarp (locations 193–195). Another fault strand is also visible ~ 50 m west of the main surface rupture. The main monoclinical scarp is traced southward through several paddy fields and dies out around location 201. From Shalabagh to Langarpura, the northwest-trending surface rupture occurs almost continuously for a distance of ~ 1 km (locations 202–251). Southwest-facing monoclinical scarps appear a few hundred meters southwest of the topographic boundary between mountains and a terrace surface. This terrace surface is the M surface, which is lower than the H surface by a few tens of meters and can be traced almost continuously upstream along the Jhelum River, as described earlier. From Shalabagh to Langarpura, the M surface appears to form a broad cumulative warp, along the base of which the surface rupture formed. Vertical separation across the 2005 rupture ranges from 0.8 m to 1.4 m along this section.

The main rupture makes an ~ 150 -m right step at the severely damaged village of Langarpura, producing complex surface rupture geometry (locations 233–251). Close to the western end of the main surface rupture, an ~ 20 -m-wide broad warp is formed in a wheat field with a vertical separation of ~ 1.75 m (location 248). South of a 2.95-m-high fault scarp at the valley bottom of the Marie di Kassel (location 252), the fault is indistinct for a distance of ~ 2 km masked by numerous landslides including a reactivated huge landslide between locations 258 and 259. Nonetheless, we found several possible surface ruptures along this section of the fault (locations 253–258). In particular, a clear southwest-facing flexure is formed at location 258 with a vertical separation of ~ 0.85 m.

The surface rupture reappears on a small saddle at location 259 and is traced southeastward on a mountain slope. From location 265, monoclinical scarps are along the base of a preexisting cumulative scarp on the M terrace surface, on which the village of Prak is situated. At the valley bottom of Prak da Katha to the southeast, a flight of two low terrace surfaces of probable Holocene age occur on the right bank of the river. The surface rupture crosses those surfaces. On the lower surface is a 3.7-m-high monoclinical scarp that is due to the 2005 earthquake only (location 270). A much larger scarp, ~ 15 -m high, is formed on the upper surface (location 269), which is clearly from multiple earthquakes, including the 2005 event. From this location to the southeast, no

clear surface rupture is observed for a distance of ~ 1.5 km primarily because of slope failures.

Khun Bandi to Malsipain (Fig. A1g, Locations 272–343)

The surface rupture becomes distinct again at Kun Bandi. Discontinuous surface rupture appears along the base of a preexisting fault warp on the M surface (locations 272–274). We found another surface rupture trace ~ 100 m southwest (locations 275–277), along which the M surface also appears to be slightly warped southwestward on the CORONA images. From locations 279 to 306, monoclinical scarps and pressure ridges are traced almost continuously for a distance of ~ 800 m along the base of a distinctive preexisting fault scarp on the M surface. Vertical separation reaches ~ 2.25 m at location 302. A short back-thrust scarp, ~ 0.5 m high, is also found on the upthrown side, ~ 100 m east of the main fault rupture (locations 283–285). South of location 306, the surface rupture appears at the valley bottom of Phulhotar da Katha. The main monoclinical scarp (location 310) as well as a south-facing minor fault scarp (location 307–309) are observed on the right bank, but no clear surface rupture is visible on the present riverbed and the left bank.

On the M surface to the south, a northwest-trending broad flexure is continuous along the base of a preexisting warp (locations 311–314). Although the preexisting warp extends further southeastward, the surface rupture deviates from the preexisting fault trace at location 314 eastward up to location 317. A vertical separation of ~ 1.05 m is measured across the monoclinical scarp on this east–west-trending short section. After making a small right step, the northwest-trending surface rupture reappears for a short distance until it encounters a shallow valley at location 319. No distinctive surface rupture is recognized at the valley bottom, however. To the southeast, a continuous southwest-facing monoclinical scarp occurs through Thotha village, following the base of a preexisting warp on the M surface (locations 320–330). Although the preexisting warp continues toward a saddle to the southeast, the surface rupture dies out around location 330, and no distinctive surface deformation was recognized north of Jandarbain Katha.

A spectacular fault scarp appears across the valley bottom of Jandarbain Katha (locations 331–332). On the left bank of the river is a low terrace surface of probable Holocene age, on which a 10- to 20-m-wide monoclinical scarp is formed continuously for a distance of ~ 100 m (Fig. 9a). The scarp trends almost north–south and is a typical pressure ridge, which is associated with rolled-up or bulldozed turf (Fig. 9b) at its base and extensive tension cracks on its crest. Vertical separation across the fault scarp is 3.4 ± 0.4 m (Fig. 9d), and simple scarp morphology implies that the vertical separation is entirely due to the 2005 earthquake. This is also supported by the CORONA satellite images, on which no distinctive preexisting scarp is recognized on

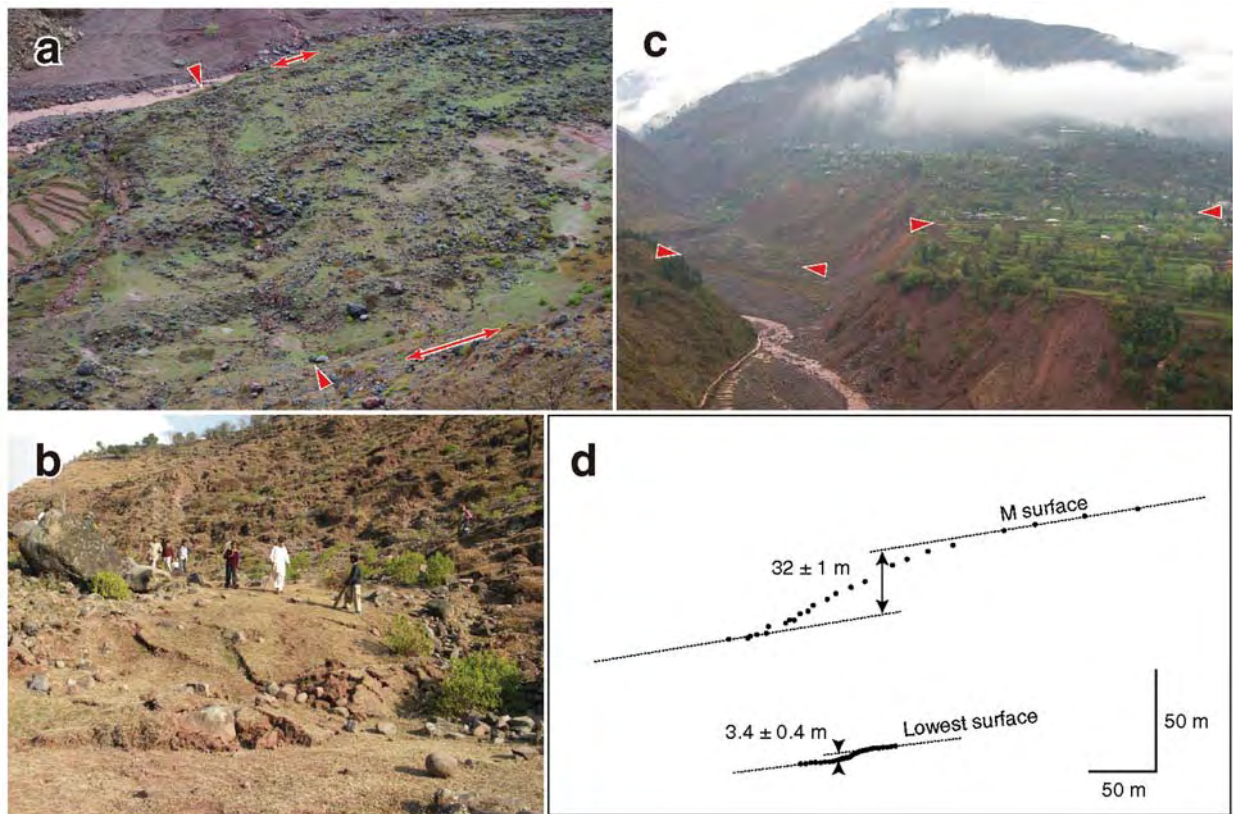


Figure 9. (a) The surface rupture across the lowest terrace surface on the left bank of Jandarbain Katha (locations 331–332). Looking north. Base of the monoclinical scarp and the zone of tension cracks on the scarp crest are indicated by arrows and double-sided arrows, respectively. Note small ponds on the farther right, which may reflect a slight back tilt. (b) Rolled-up or bulldozed turf at the base of the pressure ridge, indicating horizontal shortening, location 332. (c) Distant view of the ~32-m-high cumulative fault scarp formed on the M surface at Malsipain. Looking northeast. On the left is the valley of Jandarbain Katha. Red arrows indicate the trace of the 2005 surface rupture. (d) Topographic profiles of the cumulative fault scarp on the M surface and the 2005 fault scarp. Occurrence of 9–10 similar earthquakes after abandonment of the M surface is suggested assuming characteristic behavior.

the terrace surface. Minor right-lateral slip component is also implied by the left-stepping en echelon pattern of the tension cracks on the scarp crest. From location 331 to the north, the surface rupture crosses the present riverbed forming a small waterfall, hikes up a debris surface on the right bank for a short distance, and disappears beneath earthquake-induced landslides.

Immediately south of Jandarbain Katha, a distinctive multievent fault scarp is recognized on the M surface, on which the village of Malsipain is located (Fig. 9c; Kumahara and Nakata, 2006). Surface profiling across the scarp yields a cumulative vertical separation of 32 ± 1 m (Fig. 9d). Along the base of the preexisting scarp on the Malsipain M surface, intermittent monoclinical scarps tilted and destroyed several houses, but the amount of vertical separation is less than 1 m (locations 333–343).

South of Malsipain to Batllan Katha (Fig. A1h, Locations 344–369)

South of Malsipain, no distinctive surface rupture occurs between locations 343 and 347, although the preexisting

fault scarp/warp appears to extend southeastward. However, a newly paved road across the preexisting broad warp was buckled at several places (locations 344–346). An open fissure was also recognized around the warp crest (location 346). Amount of shortening is up to a few tens of centimeters at each site, but total shortening probably is more than a meter. We infer that the brittle pavement served as an excellent detector of broad deformation that is not identifiable on soil ground. To the southeast at location 347, we also found a slight warp in a wheat field with a vertical separation of only ~0.2 m.

A clear surface rupture appears at location 348, extending to south of location 358 with some minor gaps and steps. Southwest-facing monoclinical scarps are formed along the basal part of a preexisting warp, with vertical separation up to 1 m. Although no visible deformation occurs along the valley south of location 358, the surface rupture becomes distinct on the M surface farther south (locations 359–365). A monoclinical scarp, several tens of centimeters high, is traced continuously southeastward through numerous paddy fields, crossing an unpaved road at location 362 and deform-

ing a small culvert at location 363. The surface rupture, however, dies out around location 365. From location 365 to the southeast, southwest-facing preexisting warps are intermittently recognized for a distance of ~ 2.5 km on patchy remnants of the M surface, but we were unable to find a distinctive tectonic rupture along this section, except for a very small north-south-trending shortening feature south of Lawasi (locations 366–367).

At the valley bottom of Batllan Katha, a northwest-trending 0.8-m-high monoclinical scarp appears on a grassy surface on the left bank of the river (locations 368–369). A small rapid is also formed where the fault crosses the river. In this valley, no preexisting fault scarp is recognized in the field or on the CORONA satellite images. Although a distinctive fault scarp occurs in the valley bottom, nothing is found on the M surfaces to the northwest and southeast, both of which appear to be warped toward southwest.

North of Maira Dadu to Baghsar (Fig. A1i, Locations 370–459)

From north of Maira Dadu (location 370) to the southeast, the surface rupture is evident. Monoclinical scarps are intermittently traced along the base of a preexisting fault scarp/warp of the M surface, on which the Maira Dadu village is located (locations 370–386). Vertical separations are measured to be ~ 1.75 m across a broad warp in a wheat field (location 371), ~ 1.05 m at a dirt road in an incised valley (location 375), and ~ 2.1 m at a paved road on the M surface (location 384). Other than at those sites, the amount of vertical separation is generally not measurable, in particular where the surface rupture coincides exactly with the base of a preexisting fault scarp.

In the valley of Naushahra Katha, the surface rupture crosses the modern riverbed as well as a grass-covered surface on the left bank, several meters high (locations 387–388). A small waterfall is formed in the river whereas the grassy surface exhibits beautiful monoclinical deformation (Fig. 12a). Vertical separations are 3.2 ± 0.2 m and 3.65 ± 0.55 m for the modern and terrace surfaces, respectively, implying no preexisting scarp on the terrace surface. A continuous monoclinical scarp with left-stepping en echelon fissures on its crest is found on the M surface to the southeast (locations 389–391), with vertical separation up to ~ 1.25 m. The surface rupture coincides with the base of a preexisting warp of the terrace surface.

To the southeast, the main surface rupture makes a right step to appear on a low terrace surface on which the village of Naushahra is situated (locations 392–399). This surface stands 70–80-m lower than the M surface but 10–20-m higher than the present Jhelum River. Based on the CORONA satellite images, there is a distinctive preexisting fault scarp on this surface (Kumahara and Nakata, 2006), along the base of which the monoclinical scarp formed in 2005. The scarp gains height toward the southeast, up to ~ 1.35 -m high at the southeastern margin of the terrace sur-

face (location 399). We also found a minor thrust surface rupture ~ 250 m northeast of and subparallel to the main rupture (locations 400–402). A southeastern continuation of this rupture is also recognized on the opposite side (south bank) of the Jhelum River for a short distance (locations 403–404), where the basement of a totally destroyed house was anomalously tilted toward the southwest.

The main surface rupture crosses the Jhelum River to form a monoclinical scarp on its left bank (location 405; Fig. 10a). No distinctive rapid was recognized in the river in March 2006 probably because of quick erosion. A man-made stone wall and a dirt road are both vertically displaced by ~ 1.7 m, including a broad warp on the upthrown side (Fig. 10b). The stone wall also appears to be slightly and left-laterally offset (Ⓔ see Photo i-12 in the electronic edition of *BSSA*), but this could be an apparent offset resulting from the wall strike that is not perfectly normal to the fault trace. The surface rupture is traced almost continuously southeastward along a small stream up to location 422, although the rupture is partially covered by landslide debris shed from the northeast. From location 422, the rupture deviates from the stream, climbs across wheat fields, and dies out around location 425, where a paved road exhibits some shortening. Height of the monoclinical scarps is less than 1 m along this section of the fault. The main fault steps to the right by ~ 100 m to appear at location 427. Slight thrust scarp grows southeast to an ~ 0.55 -m-high monoclinical scarp at location 430, where a paved road and an unpaved path show clear drops. The monoclinical scarp climbs up along a small stream right toward a saddle between Dhallan and Sar Pain. On the saddle, we found no distinctive tectonic feature except for remnants of a severely damaged and uplifted paved road (location 432). Local people said that hills pushed the road from both sides of the saddle at the time of the earthquake, suggesting that considerable amount of shortening occurred here.

Prominent uphill-facing fault scarps appear at Sar Pain on the M surface (locations 435–442). On the CORONA satellite images taken in 1971, a southwest-facing cumulative fault warp is recognized on this surface, creating a local depression to the southwest (Kumahara and Nakata, 2006). A pair of ponds or swamps is visible in the depression on the CORONA images, but they were subsequently drained by a man-made channel. The 2005 surface rupture crossed and blocked the channel at location 436, leading to reestablishment of those ponds (Fig. 10c). The prominent uphill-facing scarps (locations 435–439 and 441–442) are somewhat extensional because open cracks developed at the bases of the nearly vertical scarps. Vertical separation reaches ~ 1.65 m, but no evidence of horizontal shortening is recognized. We also found a small monoclinical scarp to the southwest, extending southeastward from location 440. The monoclinical scarp disappears into the pond to the northwest. According to locals, the land between the ponds and the extensional scarps (locations 435–439) was slightly tilted toward the southwest during the earthquake. From those observations,



Figure 10. (a) Distant view of the surface rupture across the Jhelum River at Dhallan (location 405). Looking northeast. A scar indicated by arrows is a fault scarp formed during the 2005 earthquake. The fault scarp also crosses a man-made stone wall on the left bank. (b) Close-up view of the displaced man-made stone wall. Vertical separation is ~ 1.7 m including a broad warp on the upthrown side. (c) Distant view of Sar Pain (locations 435–442). Looking northwest. Uphill-facing warps and scarps reestablished the once-drained, dammed-up ponds, creating one of the most spectacular landscapes of the 2005 surface faulting. Given the probable presence of thick, fine-grained, dammed-up sediments, Sar Pain might serve as an excellent paleoseismic site for future studies. The inferred trace of the main rupture is indicated by arrows. (d) The tectonic bulge across the riverbed of Baghsar Katha (locations 455–459). Looking south. A small pool is formed immediately upstream of the surface rupture.

we infer that the main rupture passes through the ponds connecting locations 432 and 440 (Fig. 10c), although a part of the rupture does not reach the surface. The prominent extensional scarps are probably subsidiary faults developed on the upthrown side. The extensional scarps are also traced northwestward up to a hill (locations 433–435), but they could be partially gravitational.

The small monoclinical scarp continues intermittently to the southeast toward a saddle dividing Sar Pain and Baghsar (locations 440–446). A house straddling the surface rupture at location 443 is obviously tilted and seriously damaged, but barely escaped from total collapse, probably because of small vertical separation up to ~ 0.25 m.

Monoclinical scarps are identified almost continuously from immediately south of the saddle onto a tributary terrace surface of Baghsar (locations 447–454). As no name is given for this tributary on published maps, we here tentatively call it Baghsar Katha. A southwest-facing cumulative warp is recognized on this surface by the CORONA images (Kuma-

hara and Nakata, 2006). Monoclinical scarps less than 1-m high appear along the base of the preexisting warp, producing a very small pond on the downthrown side just south of location 449. The surface rupture climbs down the terrace riser southeast of location 454 and forms an impressive northwest-trending tectonic bulge traversing the modern riverbed of Baghsar Katha (locations 455–457; Fig. 10d). A small pool is also formed upstream of the bulge where it crosses the river. On the right bank, the fault extends sub-parallel to the river for a distance of ~ 100 m with a vertical separation up to ~ 1.75 m, and abruptly disappears at location 459, as it becomes covered by landslide debris. Upstream along Baghsar Katha, landslides are exclusively concentrated on its eastern slope, implying fault passage there.

Chikar Khas to Bagh (Fig. A1j, Locations 460–490)

From south of Baghsar (location 459) to the southeast, we did not conduct detailed mapping because the fault ex-

tends within mountainous terrain with numerous earthquake-induced landslides and without geomorphic evidence of active faulting (Kumahara and Nakata, 2006). We only checked along the road connecting Sar Pain and Bagh and found relatively small tectonic surface ruptures at three localities.

Immediately north of the town of Chikar Khas, we found a north-south-trending surface rupture on a north-facing slope. The rupture consists of two subparallel traces 20–30 m apart, each extending for ~200 m. The western surface rupture (locations 460–463) forms distinctive mole tracks and pressure ridges with consistent vertical separation of east side up. Although we were not able to make a reliable estimate, the vertical separation does not exceed 1 m. The eastern trace (location 464–468) appears to be primarily a strike-slip fault. Right-lateral slip of up to ~1.5 m is evident from offset features such as a trail and a man-made stone wall. Sense of vertical slip varies along the fault trace, which is commonly observed on strike-slip faults.

About 5 km southeast of Chikar Khas, northwest-trending cracks are almost continuously traced for a distance of ~500 m (location 469–487). Just south of location 469, the road connecting Chikar Khas and Sudhan Gali is ruptured where it makes a hairpin curve, forming two 10–20 cm drops down to the east. A volleyball court adjacent to the road is also warped and ruptured. To the southeast, the surface cracks cross a small bedrock mound and continue on a mountain slope and cultivated fields down to location 487. Although no systematic vertical or horizontal separation is recognized, we infer that those ruptures are at least partially tectonic in origin because they are aligned for a long distance in the direction of the earthquake fault, rather than showing a curved geometry expected for gravitational scarps.

We also found a short surface rupture of probable tectonic origin on a south-facing mountain slope just south of Sudhan Gali, a village located at the highest point of the Sar Pain-Bagh road. Continuous northwest-trending mole tracks are found on cultivated fields for a distance of ~100 m (locations 488–489). The amount of shortening is probably on the order of a few tens of centimeters, but no vertical separation is recognized across the mole tracks. Another subparallel shortening feature is recognized on a dirt road at location 490, where the road is unnaturally bulged, forming a small bump, but with no recognizable vertical separation. From here to the town of Bagh, we found some large and small ruptures on and adjacent to the road, but we interpret all those ruptures as gravitational.

Discussion

Effect of Near-Surface Geology on Measured Vertical Separation

Sixty-three vertical separation measurements are plotted along fault strike (N33°W) in Figure 11a. Measurement sites are located either on the high terraces (the H and M surfaces) or on much younger surfaces set within valleys deeply in-

cised into the high terraces. Although we could not afford to conduct a detailed investigation of the terrace deposits, our observations during the surface rupture mapping suggest that those high terraces are fill terraces with thick gravel of several tens of meters (Fig. 12a). On the contrary, the younger surfaces in the deeply incised valleys are most likely underlain by much thinner sediments. To examine the effect of near-surface geology on measured vertical separation, we use open symbols for values measured on high fill terraces and solid symbols for estimates elsewhere. The terrace surfaces exhibit systematically smaller vertical separations than the valley bottoms, in particular on the central segment. Fault scarps in the valley bottoms are typically a few times larger than those recognized on the nearby high terrace surfaces. We suggest that this is due to the absorption effect of underlying thick gravel (Fig. 12b); much of the discrete bedrock displacement is changed within the thick gravel layer to unidentifiable broad warp or tilt, and the mapped small fault scarp on the terrace surface does not represent full coseismic deformation. Complex fault branching and flattening within the gravel may also play a role in producing unidentifiable coseismic deformation. In fact, southeast of Malsipain, a newly paved road crossing the fault is buckled at several places, although no distinctive fault scarp was identified on the soil ground away from the road (locations 344–346). The brittle pavement probably records otherwise unidentifiable broad deformation.

One important implication of this absorption effect is that even though a single-earthquake broad tilt may not be identifiable, the tilt most likely becomes evident when that from multiple events is accumulated. Along some short sections of the Balakot–Bagh fault, we were unable to find evidence of surface rupture despite the presence of cumulative fault warps (e.g., southeast of location 330 and between locations 365 and 368), which is explained by the absorption effect. Our observation suggests that we cannot isolate the deformation attributed to the 2005 earthquake on the high fill terrace surface, although the cumulative warp on the surface represents the entire displacement of the buried fault. In turn, this poses caution to compare a single-earthquake fault scarp on a fill terrace surface with the larger cumulative warp standing behind.

Along-Strike Distribution of Vertical Separation

Excluding terrace surface data, we establish a slip distribution envelope by connecting the maximum values on each 2-km-long sections along the surface rupture (solid line with shade in Fig. 11a). The envelope suggests a contrasting slip distribution pattern for the northern and central segments; the northern segment shows a unimodal pattern with the maximum slip of the entire rupture on a single peak, whereas the central segment exhibits smaller slip with a multimodal or more plateaulike distribution. The unimodal distribution on the northern segment could be an artifact due to sparse measurements on this segment, but similar slip distribution is ob-

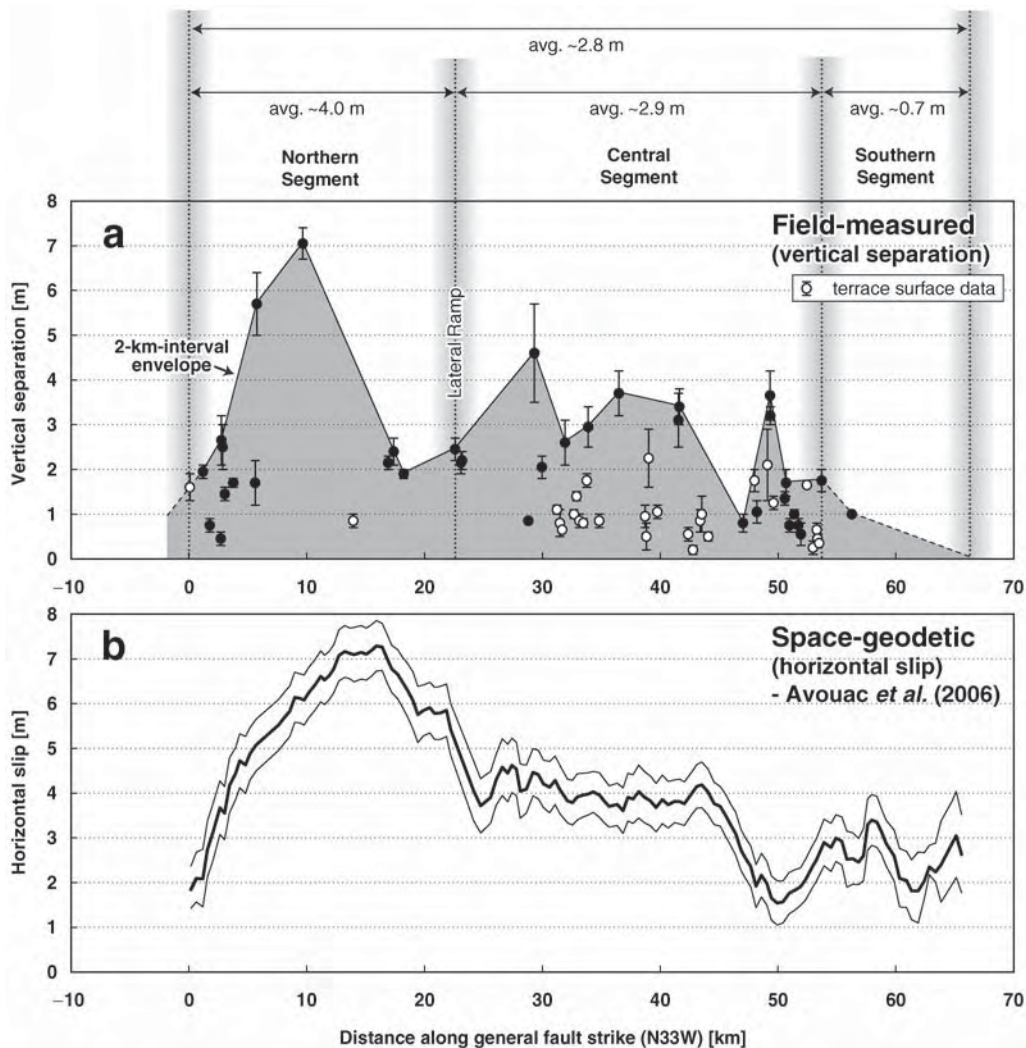


Figure 11. (a) Along-strike distribution of field-measured vertical separation. Open symbols indicate values measured on high fill terraces, whereas estimates at the valley bottoms and elsewhere are denoted by solid symbols. The terrace surface data exhibit systematically smaller vertical separations than those obtained elsewhere, suggesting the absorption effect by thick gravel fill, which is graphically explained in Fig. 12b. Solid line is a slip distribution envelope established by connecting the maximum values on each 2-km-long section along the surface rupture. (b) Along-strike distribution of horizontal slip (thick curve) and associated error (thin curves) deduced from subpixel correlation of ASTER images (Avouac *et al.*, 2006). Redrawn from original data provided by Jean-Philippe Avouac. Overall slip distribution pattern is similar to the field observation although there is a significant mismatch on the southern segment, which is probably the result of diffuse deformation and/or a smaller dip angle of the fault.

tained from subpixel correlation of ASTER images (Fig. 11b; Avouac *et al.*, 2006), although it indicates only a horizontal component of slip (mostly horizontal shortening). Good agreement between the field and space-geodetic observations indicates that the subpixel correlation technique is a powerful tool to remotely identify a surface rupture trace and its slip distribution with considerable accuracy. In fact, our horizontal shortening estimate of ~ 4.6 m north of Muzaffarabad (east of location 137), which is based on the measurement of regularly aligned fence posts, falls right between the two nearby space-geodetic estimates of 5.4 ± 0.6 m and 4.0 ± 0.7 m, which are obtained ~ 1.9 km to the west and ~ 1.3 km to the southeast, respectively. Though field observation will continue to provide essential information for in-

terpretation of tectonic geomorphic features and more details on the geometrical complexities in a fault trace that may control the rupture propagation, the subpixel correlation technique can greatly aid in time-consuming field mapping of a surface rupture if the result is provided promptly.

Avouac *et al.* (2006) ascribe the contrasting slip distribution pattern on the northern and central segments to a difference in geometric complexity of the surface rupture trace and cumulative geological displacement. However, the more sinuous and curved trace of the northern segment appears to be mostly due to topography because the segment passes through much more rugged terrain than the central segment. Alternative explanation for the contrasting distribution is a difference in bedrock geology. The northern segment mostly

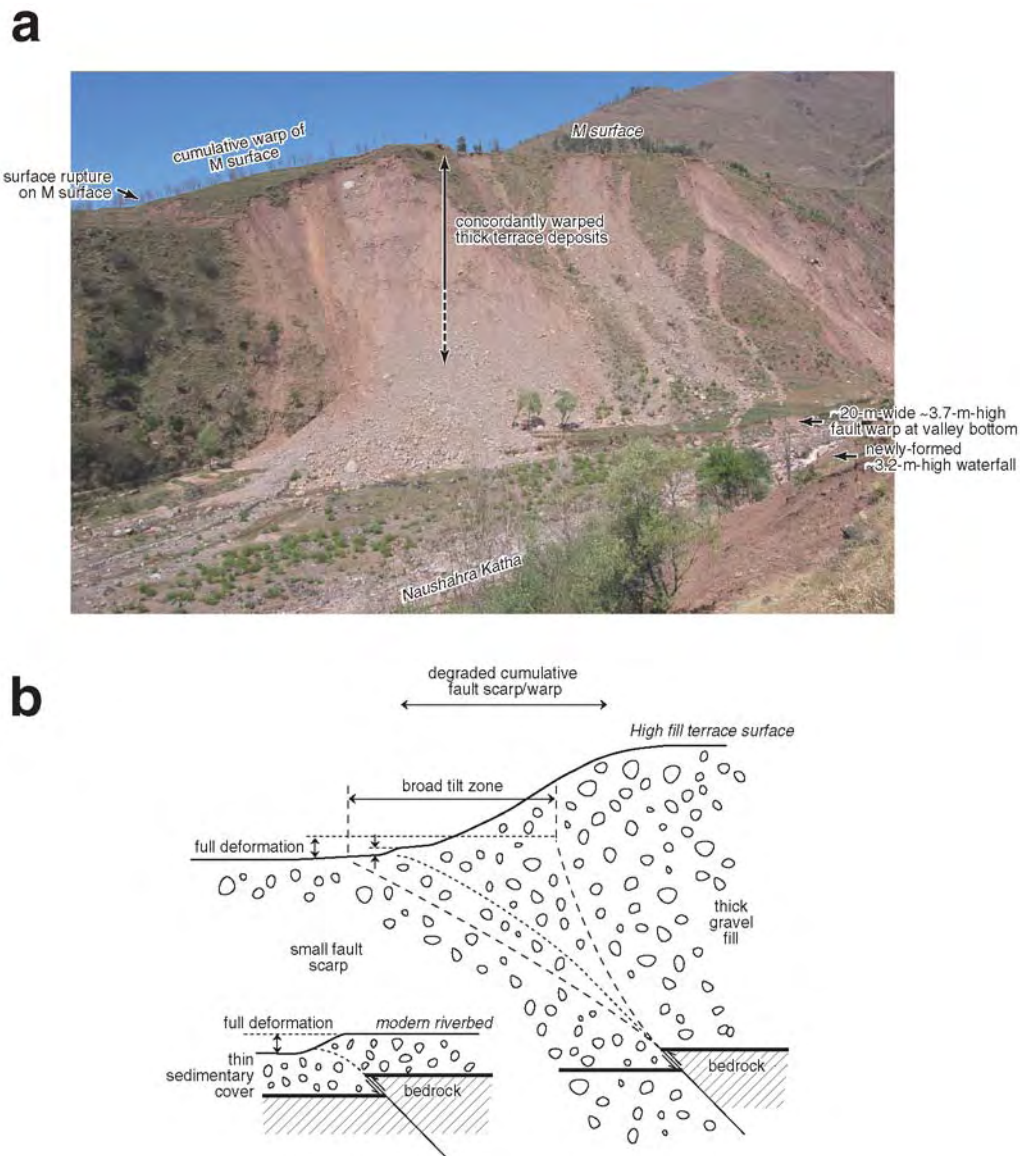


Figure 12. (a) Surface ruptures at the valley bottom of Naushahra Katha and on the M surface immediately to the northwest (locations 386–388). View north. Thick terrace deposits exposed on an ~90-m-high valley slope appears to be warped concordantly with the cumulative warp of the M surface. (b) Reason for smaller vertical separations on the high fill terrace surfaces compared with those at the valley bottoms. Discrete bedrock displacement is nearly directly expressed on the ground surface when sedimentary cover is thin (lower left). When thick gravel overlies the bedrock, much of the fault displacement is presumably changed to an unidentifiable broad warp during passing through thick gravel fill, and a recognizable small fault scarp on the terrace surface does not represent full coseismic deformation. Note that even though a single-earthquake broad tilt may not be identifiable, it most likely becomes evident when accumulated, posing caution to compare a single-earthquake fault scarp on a fill terrace surface with the larger cumulative warp standing behind.

coincides with the MBT, separating Precambrian rocks of the Lesser Himalaya from the Miocene or Precambrian rocks of the Sub-Himalaya, while the central segment extends through Miocene molasse of the Sub-Himalaya (Fig. 2). We speculate that a difference in frictional properties of the faults that arises from contrasting bedrock geology controls the maximum displacement and surface slip distribution pattern.

One big difference between our slip distribution and that of Avouac *et al.* (2006) lies on the southern segment that

extends through mountainous terrain. Avouac *et al.* (2006) shows 2–3 m of slip throughout the southern segment, whereas we found discontinuous and much smaller surface rupture with a vertical separation less than 1 m. Although we only checked along the road connecting Garhi and Bagh and could not conduct detailed mapping, the road appears to cross the surface rupture trace inferred by Avouac *et al.* (2006) several times. If the coseismic surface deformation along the southern segment localizes similarly to those along the northern and central segments, we would have found

clear continuous surface ruptures where the fault crosses the road. Given that spatial resolution of the Avouac *et al.* (2006) analysis is on the order of a few hundreds of meters, we infer that the deformation along the southern section is accommodated by small displacements on many faults distributed within a wide zone, and not concentrated on a single fault scarp; the ruptures we mapped represent only a part of the deformation. Another possible explanation is that the southern segment is a lower-angle thrust with a large horizontal shortening and a small vertical displacement. In either case, an interesting observation is that, unlike the other segments, the southern segment is devoid of geomorphic evidence of repeated surface faulting (Kumahara and Nakata, 2006). The discontinuous and small-slip surface rupture appears to be a characteristic of this section of the Balakot–Bagh fault.

Mean Vertical Displacement, Net Slip, and Horizontal Shortening

We calculated the mean vertical separation for the northern, central, and southern segments by dividing the shaded area in Fig. 11a by the segment length. The mean vertical separations are ~4.0 m, ~2.9 m, and ~0.7 m for northern, central, and southern segments, respectively. The mean for the entire rupture is estimated to be ~2.8 m. Vertical separation of a ground surface across a fault should not simply be taken as vertical fault displacement (vertical component of fault slip). Slope gradient and fault dip also affect the measured vertical separation (Fig. 13). By simple geometrical analysis assuming a constant fault dip and no strike-slip component, vertical fault displacement (VD) is written as

$$VD = VS \cdot \tan d / (\tan d + \tan s),$$

where VS is vertical separation of a ground surface, d is fault dip, and s is slope gradient. Actual near-surface fault geometry is more complex, but we assume that exclusion of deformation zones in determining vertical separations (Fig. 4) minimizes the effect of the near-surface fault complexities. Although slope gradient s is obtained from the profile, fault dip d cannot be determined without direct observation of subsurface fault geometry or measurement of multiple linear

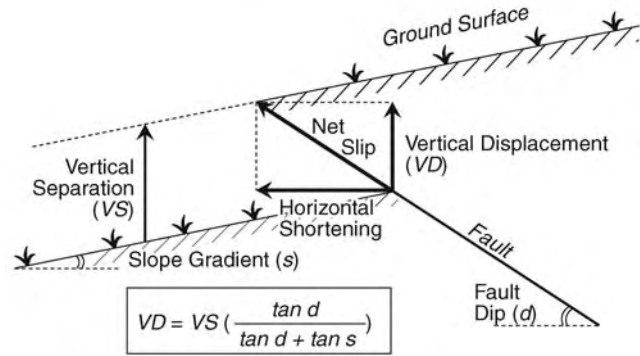


Figure 13. Schematic illustration explaining relation among vertical separation of the ground surface and various components of fault slip. Note that vertical separation of a ground surface across a fault should not be simply taken as vertical fault displacement (vertical component of fault slip), but is a function of fault dip and slope gradient in addition to vertical fault displacement. Diagram assumes a constant fault dip and a no strike-slip component of slip.

markers with different strikes crossing a fault (e.g., Sharp, 1975; Lee *et al.*, 2003). This was not attainable during our project, except for an ~3-m-deep trench excavated on the lateral ramp section north of Muzaffarabad where we found a fault dipping ~20° north (Kondo *et al.*, in preparation). We thus evaluate the effect of fault dip and slope gradient for the entire surface rupture as a whole.

Some constraints on the near-surface fault dip are geometrically obtained at several sites by comparing surface rupture locations on a terrace surface and at a valley bottom (Table 1). The obtained dip is in the range of $30 \pm 10^\circ$ with two exceptions with much smaller and larger dip values that probably reflect local fault irregularities. Near-surface fault dip determinations of $30 \pm 10^\circ$ are in good agreement with teleseismic and space-geodetic estimates of $\sim 30^\circ$ (e.g., Avouac *et al.*, 2006; Parsons *et al.*, 2006; Pathier *et al.*, 2006). On the other hand, average slope gradients of the profiles (excluding deformation zones) are mostly less than 10° with a mean of $\sim 3.7^\circ$. By using fault dip of $\sim 30^\circ$ and the average slope gradient of $\sim 3.7^\circ$, vertical fault displacement is ~10% smaller than measured vertical separation, indicating that the dip-slope effect is not significant. When this

Table 1
Geometrical Determination of Fault Dip

Site	Bank	Fault Strike Assumed	Horizontal Separation*	Height Difference*	Fault Dip
Sehli Katha	R	N30°W	~195 m	~45 m	~13°
	L	N30°W	~120 m	~45 m	~21°
Prak da Katha	R	N40°W	~120 m	~60 m	~27°
Jandarbain Katha	L	N10°W	~45 m	~65 m	~55°
Naushahra Katha	R	N45°W	~130 m	~90 m	~35°
	L	N45°W	~130 m	~95 m	~36°

*Relative location and height of surface ruptures are determined by an ordinary portable GPS receiver.

minor effect is taken into account, the mean vertical separation of ~ 2.8 m is converted to a mean vertical fault displacement of ~ 2.5 m. Ignoring the minor strike-slip component, the fault dip of $\sim 30^\circ$ then yields a mean horizontal shortening of ~ 4.3 m and mean net slip of ~ 5.0 m. Those figures are comparable to a mean horizontal shortening estimate of ~ 4.2 m from ASTER images (Avouac *et al.*, 2006) and a mean net slip estimate of ~ 5.1 m from teleseismic, SAR, and GPS observations (Bendick *et al.*, 2007).

Comparison with Seismological and Geodetic Source Models

The hypocenter determined by the USGS suggests that the rupture initiated at the deep portion of the northern-central segment boundary and propagated bilaterally to eventually break the three segments (Fig. 3). The surface slip distribution shown in Fig. 11 implies the presence of two major asperities that correspond to northern and central segments: the northern segment is a simple large-slip asperity, whereas the central segment is a larger-sized but smaller-slip asperity or a composite of multiple smaller asperities. The southern segment is probably associated with a minor asperity with even smaller slip. The fault slip model deduced from teleseismic inversion (Parsons *et al.*, 2006) shows two major asperities with the hypocenter in between, with the northern asperity relatively compact but associated with larger slip and the larger southern asperity with smaller slip. Although the asperities are set too far apart in their model, the overall slip distribution is in good agreement with our observations. Fault models inverted from surface deformation field obtained by subpixel correlation of the Envisat SAR images (Fujiwara, Tobita, Sato, Ozawa, and Une, 2006; Pathier *et al.*, 2006) give somewhat different solutions but also suggest two or multiple asperities.

In contrast, the Avouac *et al.* (2006) joint inversion model using teleseismic observations and the along-strike surface slip deduced from ASTER images suggests a single asperity just above the hypocenter. However, they assume a segment boundary (slip is 0) in the middle of our northern segment where surface displacement is largest, which probably distorts the source image. The model derived solely from teleseismic records thus shows significant misfit with the surface observations, in particular on our northern segment. To correct this misfit, Avouac *et al.* (2006) increased slips on shallowest subfaults that have the slightest impact on teleseismic waveforms. The consequence is a clear mismatch or detachment between the shallowest and deeper parts of the source fault, which appears to be unrealistic. Although their model is one solution to explain observed surface deformation and teleseismic waveforms, we prefer the two-asperity or multiple-asperity model and conclude that the surface observation reflects source process and can be used to construct source models of coming earthquakes.

Preliminary Earthquake Recurrence and Contribution to Himalayan Convergence

Many lines of geomorphic evidence document repeated surface rupture along the trace of the Balakot–Bagh fault. Although estimates of earthquake recurrence and slip rate are not the focus of this article, our field observation provides some constraint on them.

As mentioned in the detailed description of the surface rupture, the M terrace surface is cumulatively deformed by 32 ± 1 m at Malsipain, while the 2005 vertical separation is measured at 3.4 ± 0.4 m at the closest valley bottom of Jandarbain Katha (Fig. 9). Assuming characteristic behavior, these observations suggest 9–10 similar surface-rupturing earthquakes on the Balakot–Bagh fault after abandonment of the M surface. Unfortunately, we do not have any numerical age constraint on the surface to date. However, the M surface is an extensive valley-fill surface composed of thick gravel of several tens of meters, which is deeply incised by younger surfaces of probable Holocene age. As the Balakot–Bagh fault has no control on distribution of the M surface, the surface is primarily nontectonic in origin, probably reflecting regional valley-fill/downcutting history modulated by regional climatic changes.

Previous studies suggest that the last glacial maximum (LGM) in the western Himalaya, including Nanga Parbat northeast of the meizoseismal area (Fig. 1), was not synchronous with the global LGM of marine oxygen isotope stage (MIS) 2, but during MIS 3 (60–30 ka), when a stronger south Asian summer monsoon would have caused higher snowfalls at high altitudes, allowing glaciers to advance despite relatively high temperature as compared to MIS 2 (e.g., Benn and Owen, 1998; Phillips *et al.*, 2000; Richards *et al.*, 2000). Following deglaciation was primarily a period of valley fill, as is best represented at Chitral, eastern Hindu Kush, ~ 220 km northwest of the meizoseismal area, where episodes of extensive valley fill are reported between the regional LGM of MIS 3 and subsequent smaller glacial advance in late-MIS 2/early Holocene (Owen *et al.*, 2002; Kamp *et al.*, 2004). This is probably a combined effect of resedimentation of tills from the last major glaciation, increase of sediment yield through enhanced and expanded periglacial processes under the colder climate of MIS 2, and decrease of stream power due to the weakened monsoon. The incision rate and stream power of the Indus river are reported to have significantly increased after 13–15 ka (Leland *et al.*, 1998), which appears to be related to the restrengthened Asian monsoon that is responsible for the late-MIS 2/early Holocene glacial advance. Although the Jhelum river is under somewhat different environments with no contemporary glacier within its catchment, we infer that the regional climatic changes worked in a similar way and estimated the abandonment age of the M surface to be in the range of 10–30 ka.

The M surface abandonment at 10–30 ka yields the earthquake recurrence of 1000–3300 yr on the Balakot–Bagh fault. When combined with the 2005 mean slips, the mean

rates of vertical slip, horizontal shortening, and net slip on the fault are calculated to be 0.8–2.4, 1.4–4.1, and 1.6–4.7 mm/yr, respectively. The horizontal shortening rate across the Balakot–Bagh fault is only 7%–27% of the shortening across the Himalaya of 15–20 mm/yr. Although more detailed study with numerical age constraints are necessary for more reliable estimates of earthquake recurrence and slip rates, our preliminary analysis suggests that the Balakot–Bagh fault is not a main player of Himalayan contraction accommodation, causing earthquakes with a recurrence longer than a millennium.

The 2005 earthquake occupied the transitional zone between the northwest-trending Himalaya arc and east–west-trending Hazara arc (Fig. 1, inset). Strike of the causative Balakot–Bagh fault indicates that the fault is a member of the Himalaya arc, which further extends to northwest beyond the Hazara–Kashmir syntaxis as the IKSZ (Fig. 1; Armbruster *et al.*, 1978; Seeber and Armbruster, 1979). At similar longitudes to the south, the east–west-trending SRT, a main player of the Hazara arc, is taking up north–south shortening of at least 9–14 mm/yr (Baker *et al.*, 1988). The Balakot–Bagh fault and the IKSZ thus may be interpreted as the dying-out parts of the Himalaya arc, much of its contraction being accommodated by the Hazara arc represented by the SRT at these longitudes.

Irrespective of slip rate of the Balakot–Bagh fault, mean coseismic horizontal shortening of ~4.3 m indicates that the earthquake released strain equivalent to 200–300 yr of gross Himalayan strain. However, no large historical earthquake is known on this section of the Frontal Himalaya, except for possibly the A.D. 25 Taxila earthquake (e.g., Quittmeyer and Jacob, 1979); Taxila is an ancient town immediately west of Islamabad. Although the Himalayan history of large earthquakes is obviously not complete, in particular for the first millennium, a relatively large number of recorded earthquakes after the sixteenth century (Quittmeyer and Jacob, 1979) may indicate that significant earthquakes such as the 1555 and 2005 earthquakes are not missing from the historical records for the last five centuries. If so, the observation suggests that the accumulated strain was not fully released by the deadly 2005 earthquake. Although the amount of remaining strain is unknown, it may be released by another earthquake on the SRT or an active fault elsewhere. Alternatively, the strain could be accommodated by aseismic slip on the SRT due to presence of ductile salt (e.g., Yeats *et al.*, 1984).

Implications for Seismic Hazard Assessment in the Himalaya and Elsewhere

The Kashmir earthquake of 2005 was the first historical earthquake in the Himalaya known to be accompanied by surface rupture (e.g., Bilham, 2004), although paleoseismic studies suggest surface faulting during prehistoric large earthquakes on the MFT (e.g., Lavé *et al.*, 2005; Kumar *et al.*, 2006). The 2005 earthquake confirmed that earthquakes on relatively minor faults north of the MFT are also capable

of destructive surface-rupturing earthquakes. The fact that many of the 2005 ruptures reactivated previously unrecognized faults indicates the need for a search in this zone for evidence for surface rupture on prehistoric earthquakes, or even historical earthquakes such as the 1555 Srinagar and 1905 Kangra earthquakes to the east. This would allow earthquakes in this zone to be factored into a hazard assessment as a critical component, because the 2005 earthquake resulted in the greatest loss of life of any historical Himalayan earthquake, including those on the Himalayan front.

However, our experience mapping the 2005 surface rupture shows that this task will not be straightforward, in large part due to the mountainous terrain. We were unable to map surface rupture in much of the mountainous part of the meizoseismal area because of the massive landslides triggered by the earthquake on and close to the fault trace. Our best results were on streams and high terraces crossing the fault, which have the best potential for preservation as either fault scarps or broad warps. Great care thus should be taken not to miss slightest tectonic signals on young and old terrace surfaces when searching for evidence for prehistoric surface faulting.

We also note that severe structural damage was exclusively concentrated on the hanging-wall side of the thrust surface rupture at many places (e.g., Fig. 5a). This is probably a combined effect of unusually strong ground motion resulting from geometrical asymmetry of the fault with respect to the free surface (e.g., Allen *et al.*, 1998; Oglesby *et al.*, 1998; Brune *et al.*, 2004) and extensive ground deformation due to surface faulting (Kelson *et al.*, 2001). Although similar observations have been reported during historical thrust events (e.g., Iida, 1978, from the 1945 Mikawa earthquake, Japan; Kelson *et al.*, 2001, from the 1999 Chi-Chi earthquake, Taiwan), the 2005 earthquake provides one of the clearest examples of the hanging-wall devastation. The clear contrast appears to be related to the fact that the Balakot–Bagh fault extends through mountainous terrain, unlike many active thrusts that mark mountain fronts. Similar underlying geology across the fault probably minimized difference in the site effect, making the contrast clearer, as is simulated by lattice particle modeling (Shi and Brune, 2005). Seismic hazard assessment of an active thrust needs to take into account severe structural damage on the hanging wall, both from unusually strong ground motion and extensive ground deformation due to surface thrusting.

Conclusions

The 2005 M_w 7.6 Kashmir earthquake was accompanied by an ~70-km-long northwest-trending thrust surface rupture with a vertical separation up to ~7 m. Mapped surface rupture trace shows that neither the MFT nor the MBT is responsible for the earthquake, but three active faults or fault segments within the Sub-Himalaya, collectively called the Balakot–Bagh fault, make up the causative fault. The fault

locally coincides with the surface trace of the MBT, but with the opposite sense of separation.

We found that fault scarps on high fill terrace surfaces are significantly smaller than those at the bottoms of nearby incised valleys, suggesting that much of the discrete bedrock displacement is changed within the thick gravel layer to unidentifiable broad warp or tilt. Since the broad warp probably becomes evident when accumulated, this observation poses caution to compare a single-earthquake fault scarp on a fill terrace surface with the larger cumulative warp standing behind.

The surface rupture is subdivided into three geometric segments separated by small steps. Excluding fill terrace data, the mean vertical separations of the northern, central, and southern segments are ~ 4.0 m, ~ 2.9 m, and ~ 0.7 m, respectively. The mean for the entire rupture is ~ 2.8 m. When the effect of fault dip and slope gradient on measured vertical separation is taken into account, mean vertical displacement, horizontal shortening, and net slip of the entire rupture are estimated to be ~ 2.5 m, ~ 4.3 m, and ~ 5.0 m, respectively, assuming a fault dip of $\sim 30^\circ$ and a negligible minor strike-slip component.

Slip distribution along the surface rupture is in good agreement with that obtained from space-geodetic observation, with a unimodal pattern on the northern segment and a more plateaulike distribution on the central segment. The contrasting distribution may result from difference in bedrock geology through which the fault passes. The location of the hypocenter, together with seismological and geodetic source models, suggests that the rupture initiated at the deep portion of the northern-central segment boundary and propagated bilaterally to break two major asperities corresponding to the northern and central segments as well as a minor asperity corresponding to the southern segment.

Assuming that the extensive fill terrace surface, the M surface, is related to a period of deglaciation and valley fill (10–30 ka) between the regional last glacial maximum of MIS 3 and the subsequent smaller glacial advance of late-MIS 2/early Holocene, the earthquake recurrence on the Balakot–Bagh fault is estimated to be 1000–3300 yr. The rate of horizontal shortening across the fault is calculated to be 1.4–4.1 mm/yr, which is only a portion of the shortening across the Himalaya of 15–20 mm/yr. Although more detailed study with numerical age constraints is necessary, our preliminary analysis suggests that the Balakot–Bagh fault is not a main player of Himalayan contraction accommodation, causing earthquakes with a recurrence longer than a millennium. The Balakot–Bagh fault may be interpreted as a part of the Himalaya arc that is dying out; much of its contraction at these longitudes is being accommodated by the Hazara arc represented by the SRT to the south.

The mean coseismic horizontal shortening of ~ 4.3 m is equivalent to 200–300 yr of gross Himalayan strain. Assuming that no significant earthquake is missing from the historical records at least since the sixteenth century, the accumulated strain was not fully released by the 2005 earth-

quake. The remaining strain may be released by another earthquake on the SRT or an active fault elsewhere, although accommodation by aseismic slip on the SRT is another possibility.

The 2005 earthquake was not only the first historical surface-rupturing earthquake in the Himalaya, but the most devastating earthquake known to have occurred in the region. Our results indicate the potential for devastating surface-rupturing earthquakes north of the frontal thrusts and the need for a search in this zone for evidence for active faulting. We also note that severe structural damage was exclusively concentrated on the hanging-wall side of the thrust surface rupture, which is probably a combined effect of unusually strong ground motion and extensive ground deformation.

Note Added in Proof

After the submission of this manuscript, authors Nakata and Wesnousky, who were visiting the 2005 meizoseismal area for trenching and eyewitness interviews in March 2007, happened to find that the surface rupture further extends northward for a distance of ~ 1.4 km along Jalora Katha. The traces of the newly found surface rupture, together with the additional GPS-located points (locations a1–a7), $\text{\textcircled{E}}$ are added to Figure A1a and the ArcGIS files of the electronic edition of *BSSA*. The vertical separation across the fault is 0.5–2 m down to the west, but most of the fault scarp has been eroded away by floods after the earthquake (between locations a2 and a3). We also found a nearly vertical fault contact exposed at location a3, which separates the Murree formation on the east from the colluvial sediments on the west. Although the discovery of the northernmost surface rupture is important to place the northern end of the 2005 surface faulting, we note that it has little impact on the conclusions of the article, including the calculation of mean slips.

Acknowledgments

We thank Mirza Shahid Baig for discussions in the field. Gratitude is also due to Yasuhiro Kumahara for preparing enlarged stereo-paired CORONA satellite images; Mikio Tobita, Satoshi Fujiwara, and Shinzaburo Ozawa for providing unpublished surface deformation data from Envisat SAR images; Hiroshi P. Sato for providing unpublished landslide distribution data from Satellite Pour l'Observation de la Terre (SPOT) images; Jean-Philippe Avouac for providing surface slip distribution data from ASTER images; and Minoru Urai for providing DEMs from ASTER images. Aamir Rashid and Wiley Thompson kindly allowed us to use their photographs. We also thank Yuji Yagi for discussions and comments on teleseismic inversions, Daisaku Kawabata for professional support on GIS, and Yuko Ono and Eriko Maeda for technical assistance in creating figures and ArcGIS files. This paper was greatly improved by constructive comments and suggestions by two reviewers, J-P. Avouac and M. Meghraoui, and the associate editor, Eugene Schweig. This work was supported by the Active Fault Research Center, the Geological Survey of Japan, National Institute of Advanced Industrial Science and Technology (AIST), the Geological Survey of Pakistan, Earth Consultants International Inc., and Kyoto University Active Geosphere Investigations for the Twenty-First Century Centers of Excellence Program (KAGI21), which was approved by the Ministry of Education, Culture, Sports, Science, and Technology (MEXT) of Japan.

References

- Akhtar, S. S., G. Saeed, and A. Hussain (2004). Geological map of the Rawalakot area, Bagh and Rawalakot districts, AJK, Geological Map Series, Vol. 6, no. 20, Geological Survey of Pakistan, Quetta, Sheet No. 43 G/13, scale 1:50,000.
- Akhtar, S. S., Waliullah, A. Hussain, and R. M. N. Khan (2004). Geological map of the Dhirkot area, Muzaffarabad and Bagh districts, AJK, and parts of Rawalpindi and Abbottabad districts, NWFP, Pakistan, Geological Map Series, Vol. 6, no. 16, Geological Survey of Pakistan, Quetta, Sheet No. 43 F/12, scale 1:50,000.
- Allen, C. R., J. N. Brune, L. S. Cluff, and A. G. Barrows Jr. (1998). Evidence for unusually strong near-field ground motion on the hanging wall of the San Fernando fault during the 1971 earthquake, *Seism. Res. Lett.* **69**, 524–531.
- Ambraseys, N., and D. Jackson (2003). A note on early earthquakes in northern India and southern Tibet, *Curr. Sci.* **84**, 570–582.
- Anwar, C. M., A. I. Bhutta, and A. Hussain (2004). Geological map of the Chakothi area, districts Muzaffarabad and Punch, AJK, Geological Map Series, Vol. 6, no. 17, Geological Survey of Pakistan, Quetta, Sheet No. 43 F/16, scale 1:50,000.
- Armbruster, J., L. Seeber, and K. H. Jacob (1978). The northwestern termination of the Himalayan mountain front: active tectonics from micro-earthquakes, *J. Geophys. Res.* **83**, 269–281.
- Avouac, J.-P., F. Ayoub, S. Leprince, O. Konea, and D. V. Helmberger (2006). The 2005 M_w 7.6 Kashmir earthquake: sub-pixel correlation of ASTER images and seismic waveforms analysis, *Earth Planet. Sci. Lett.* **249**, 514–528.
- Baig, M. S. (2006). Active faulting and earthquake deformation in Hazara-Kashmir syntaxis, Azad Kashmir, northwest Himalaya, Pakistan, in *International Conference on Earthquake in Pakistan, Extended Abstracts*, A. B. Kausar, T. Karim and T. Khan (Editors), Geological Survey of Pakistan, Quetta, 21–22.
- Baker, D. M., R. J. Lillie, R. S. Yeats, G. D. Johnson, M. Yousuf, and A. S. H. Zamin (1988). Development of the Himalayan frontal thrust zone: Salt Range, Pakistan, *Geology* **16**, 3–7.
- Banerjee, P., and R. Bürgmann (2002). Convergence across the northwest Himalaya from GPS measurements, *Geophys. Res. Lett.* **29**, 1652, doi 10.1029/2002GL015184.
- Bendick, R., R. Bilham, M. A. Khan, and S. F. Khan (2007). Slip on an active wedge thrust from geodetic observations of the 8 October 2005 Kashmir earthquake, *Geology* **35**, 267–270.
- Benn, D. I., and L. A. Owen (1998). The role of the Indian summer monsoon and the mid-latitude westerlies in Himalayan glaciation: review and speculative discussion, *J. Geol. Soc. Lond.* **155**, 353–363.
- Bettinelli, P., J.-P. Avouac, M. Flouzat, F. Jouanne, L. Bollinger, P. Willis, and G. R. Chitrakar (2006). Plate motion of India and interseismic strain in the Nepal Himalaya from GPS and DORIS measurements, *J. Geod.* **80**, 567–589.
- Bilham, R. (2004). Earthquakes in India and the Himalaya: tectonics, geodesy and history, *Ann. Geophys.* **47**, 839–858.
- Bilham, R., V. K. Gaur, and P. Molnar (2001). Himalayan seismic hazard, *Science* **293**, 1442–1444.
- Bilham, R., K. Larson, J. Freymueller, F. Jouanne, P. Le Fort, P. Leturmy, J. L. Mugnier, J. F. Gamond, J. P. Glot, J. Martinod, N. L. Chaudury, G. R. Chitrakar, U. P. Gautam, B. P. Koirala, M. R. Pandey, R. Ranabhat, S. N. Sapkota, P. L. Shrestha, M. C. Thakuri, U. R. Timilsina, D. R. Tiwari, G. Vidal, C. Vigny, A. Galy, and B. de Voogd (1997). GPS measurements of present-day convergence across the Nepal Himalaya, *Nature* **386**, 61–64.
- Brune, J. N., A. Anoshheepoor, B. Shi, and Y. Zeng (2004). Precarious rock and overturned transformer evidence for ground shaking in the M_s 7.7 Kern County earthquake: an analog for disastrous shaking from a major thrust fault in the Los Angeles basin, *Bull. Seismol. Soc. Am.* **94**, 1993–2003.
- Burg, J.-P., B. Celerier, N. M. Chaudhry, M. Ghazanfar, F. Gnehm, and M. Schnellmann (2005). Fault analysis and paleostress evolution in large strain regions: methodological and geological discussion of the south-eastern Himalayan fold-and-thrust belt in Pakistan, *J. Asian Earth Sci.* **24**, 445–467.
- Calkins, J. A., A. S. A. Matin, A. Hussain, M. N. Mughal, I. Haq, and A. Latif (2004). Geological map of the Garhi Habibullah area, district Mansehra and parts of Muzaffarabad district, AJK, Geological Map Series Vol. 6, no. 13, Geological Survey of Pakistan, Quetta, Sheet No. 43 F/7, scale 1:50,000.
- Calkins, J. A., T. W. Offield, S. K. M. Abdullah, and S. T. Ali (1975). Geology of the southern Himalaya in Hazara, Pakistan, and adjacent areas, *U.S. Geol. Surv. Profess. Pap.* 716-C.
- DeMets, C., R. G. Gordon, D. F. Argus, and S. Stein (1990). Current plate motions, *Geophys. J. Int.* **101**, 425–478.
- DeMets, C., R. G. Gordon, D. F. Argus, and S. Stein (1994). Effect of recent revisions to the geomagnetic reversals time scale on estimates of current plate motions, *Geophys. Res. Lett.* **21**, 2191–2194.
- Fujiwara, S., M. Tobita, H. P. Sato, S. Ozawa, and H. Une (2006). Crustal deformation and earthquake fault of the 2005 northern Pakistan earthquake detected by spaceborne synthetic aperture radar, *E-J. GEO* **2**, 95–103 (in Japanese with English abstract).
- Fujiwara, S., M. Tobita, H. P. Sato, S. Ozawa, H. Une, M. Koarai, H. Nakai, M. Fujiwara, H. Yurai, T. Nishimura, and F. Hayashi (2006). Satellite data gives snapshot of the 2005 Pakistan earthquake, *EOS Trans.* **87**, 73–77.
- Hussain, A., and R. S. Yeats (2006). The Balakot–Bagh fault that triggered the October 8, earthquake and other active faults in the Himalayan foreland region, Pakistan, in *International Conference on Earthquake in Pakistan: Extended Abstracts*, A. B. Kausar, T. Karim and T. Khan (Editors), Geological Survey of Pakistan, Quetta, 115–116.
- Iida, K. (1978). Report of the earthquake section of the Disaster Prevention Committee, in *Distribution of earthquake damage and seismic intensity caused by the Mikawa earthquake of January 13, 1945*, Earthquake Section of the Disaster Prevention Committee, Aichi Prefecture, Japan, 96 pp. (in Japanese).
- Iqbal, S., S. Nasir, and A. Hussain (2004). Geological map of the Nauseri area, district Muzaffarabad, AJK, Geological Map Series Vol. 6, no. 14, Geological Survey of Pakistan, Quetta, Sheet No. 43 F/11, scale 1:50,000.
- Kamp, U., Jr., K. Haserodt, and J. F. Shroder Jr. (2004). Quaternary landscape evolution in the eastern Hindu Kush, Pakistan, *Geomorphology* **57**, 1–27.
- Kelson, K. I., K.-H. Kang, W. D. Page, C.-T. Lee, and L. S. Cluff (2001). Representative styles of deformation along the Chelungpu fault from the 1999 Chi-Chi (Taiwan) earthquake: geomorphic characteristics and responses of man-made structures, *Bull. Seismol. Soc. Am.* **91**, 930–952.
- Khattari, K. N. (1987). Great earthquakes, seismicity gaps and potential for earthquake disaster along the Himalaya plate boundary, *Tectonophysics* **138**, 79–92.
- Kumahara, Y., and T. Nakata (2006). Special Publication 41, Active faults in the epicentral area of the 2005 Pakistan earthquake, Research Center for Regional Geography, Hiroshima University, Hiroshima.
- Kumar, S., S. G. Wesnousky, T. K. Rockwell, D. Regona, V. C. Thakur, and G. G. Seitz (2001). Earthquake recurrence and rupture dynamics of Himalayan Frontal thrust, India, *Science* **294**, 2328–2331.
- Kumar, S., S. G. Wesnousky, T. K. Rockwell, R. W. Briggs, V. C. Thakur, and R. Jayangondaperumal (2006). Paleoseismic evidence of great surface rupture earthquakes along the Indian Himalaya, *J. Geophys. Res.* **111**, B03304, doi 10.1029/2004JB003309.
- Lavé, J., and J. P. Avouac (2000). Active folding of fluvial terraces across the Siwaliks Hills, Himalayas of central Nepal, *J. Geophys. Res.* **105**, 5735–5770.
- Lavé, J., D. Yule, S. Sapkota, K. Basant, C. Madden, M. Attal, and R. Pandey (2005). Evidence for a great medieval earthquake in the central Himalayas, Nepal, *Science* **307**, 1302–1305.
- Lee, Y.-H., M.-L. Hsieh, S.-D. Lu, T.-S. Shih, W.-Y. Wu, Y. Sugiyama, T. Azuma, and Y. Kariya (2003). Slip vectors of the surface rupture of

- the 1999 Chi-Chi earthquake, western Taiwan, *J. Struct. Geol.* **25**, 1917–1931.
- Leland, J., M. R. Reid, D. W. Burbank, R. Finkel, and M. Caffee (1998). Incision and differential bedrock uplift along the Indus River near Nanga Parbat, Pakistan Himalaya, from ^{10}Be and ^{26}Al exposure age dating of bedrock straths, *Earth Planet. Sci. Lett.* **154**, 93–107.
- Nakata, T. (1989). Special Paper 232, Active faults of the Himalaya of India and Nepal, in *Tectonics of the Western Himalayas*, L. L. Malinconico Jr. and R. J. Lillie (Editors), Geological Society of America, Boulder, Colorado, 243–264.
- Nakata, T., H. Tsutsumi, S. H. Khan, and R. D. Lawrence (1991). Special publication 21, Active faults of Pakistan: map sheets and inventories, Research Center for Regional Geography, Hiroshima University, Hiroshima.
- Oglesby, D. D., R. J. Archuleta, and S. B. Nielsen (1998). Earthquakes on dipping faults: the effect of broken symmetry, *Science* **280**, 1055–1059.
- Owen, L. A., U. Kamp, J. Q. Spencer, and K. Haserodt (2002). Timing and style of late Quaternary glaciation in the eastern Hindu Kush, Chitral, northern Pakistan: a review and revision of the glacial chronology based on new optically stimulated luminescence dating, *Quat. Int.* **97–98**, 41–55.
- Parsons, T., R. S. Yeats, Y. Yagi, and A. Hussain (2006). Static stress change from the 8 October, 2005 $M = 7.6$ Kashmir earthquake, *Geophys. Res. Lett.* **33**, L06304, doi 10.1029/2005GL025429.
- Pathier, E., E. J. Fielding, T. J. Wright, R. Walker, B. E. Parsons, and S. Hensley (2006). Displacement field and slip distribution on the 2005 Kashmir earthquake from SAR imagery, *Geophys. Res. Lett.* **33**, L20310, doi 10.1029/2006GL027193.
- Pennington, W. D. (1979). A summary of field and seismic observations of the Pattan earthquake: 28 December 1974, in *Geodynamics of Pakistan*, A. Farah and K. A. DeJong (editors), Geological Survey of Pakistan, Quetta, 143–147.
- Philip, H., and M. Meghraoui (1983). Structural analysis and interpretation of the surface deformations of the El Asnam earthquake of October 10, 1980, *Tectonics* **2**, 17–49.
- Philip, H., E. Rogozhin, A. Cisternas, J. C. Bousquet, B. Borisov, and A. Karakhanian (1992). The Armenian earthquake of 1988 December 7: faulting and folding, neotectonics and paleoseismicity, *Geophys. J. Int.* **110**, 141–158.
- Phillips, W. M., V. F. Sloan, J. F. Shroder Jr., P. Sharma, M. L. Clarke, and H. M. Rendell (2000). Asynchronous glaciation at Nanga Parbat, northwestern Himalaya mountains, Pakistan, *Geology* **28**, 431–434.
- Quittmeyer, R. C., and K. H. Jacob (1979). Historical and modern seismicity of Pakistan, Afghanistan, northwestern India, and southeastern Iran, *Bull. Seismol. Soc. Am.* **69**, 773–823.
- Richards, B. W., L. A. Owen, and E. J. Rhodes (2000). Timing of late Quaternary glaciations in the Himalayas of northern Pakistan, *J. Quat. Sci.* **15**, 283–297.
- Rubin, C. (1996). Systematic underestimation of earthquake magnitudes from large intracontinental reverse faults: historical ruptures break across segment boundaries, *Geology* **24**, 989–992.
- Seeber, L., and J. Armbruster (1979). Seismicity of the Hazara arc in northern Pakistan: decollement vs. basement faulting, in *Geodynamics of Pakistan*, A. Farah and K. A. DeJong (Editors), Geological Survey of Pakistan, Quetta, 131–142.
- Sella, G., T. H. Dixon, and A. Mao (2002). REVEL: a model for recent plate velocities from space geodesy, *J. Geophys. Res.* **107**, 2081, doi 10.1029/2000JB000033.
- Sharp, R. V. (1975). Displacement on tectonic ruptures, *Calif. Div. Mines Geol. Bull.* **196**, 187–194.
- Shi, B., and J. N. Brune (2005). Characteristics of near-fault ground motions by dynamic thrust faulting: two-dimensional lattice particle approaches, *Bull. Seismol. Soc. Am.* **95**, 2525–2533.
- Tapponnier, P., G. King, and L. Bollinger (2006). Active faulting and seismic hazard in the western Himalayan syntaxis, Pakistan, in *International Conference on Earthquake in Pakistan: Extended Abstracts*, A. B. Kausar, T. Karim and T. Khan (Editors), Geological Survey of Pakistan, Quetta, 2–3.
- Tapponnier, P., G. King, L. Bollinger, and J. Grasso (2006). Surface faulting during the October 8th, 2005, Muzaffarabad earthquake and Coulomb stress increase on the Jhelum fault, *Seism. Res. Lett.* **77**, 234.
- Yeats, R. S., A. B. Kausar, and T. Nakata (2006). Conferees examine deadly 2005 Kashmir earthquake, *EOS* **87**, 115.
- Yeats, R. S., S. H. Khan, and M. Akhtar (1984). Late Quaternary deformation of the Salt Range of Pakistan, *Geol. Soc. Am. Bull.* **95**, 958–966.

Appendix

Figure A1 shows detailed maps of the surface rupture associated with the 2005 Kashmir earthquake.

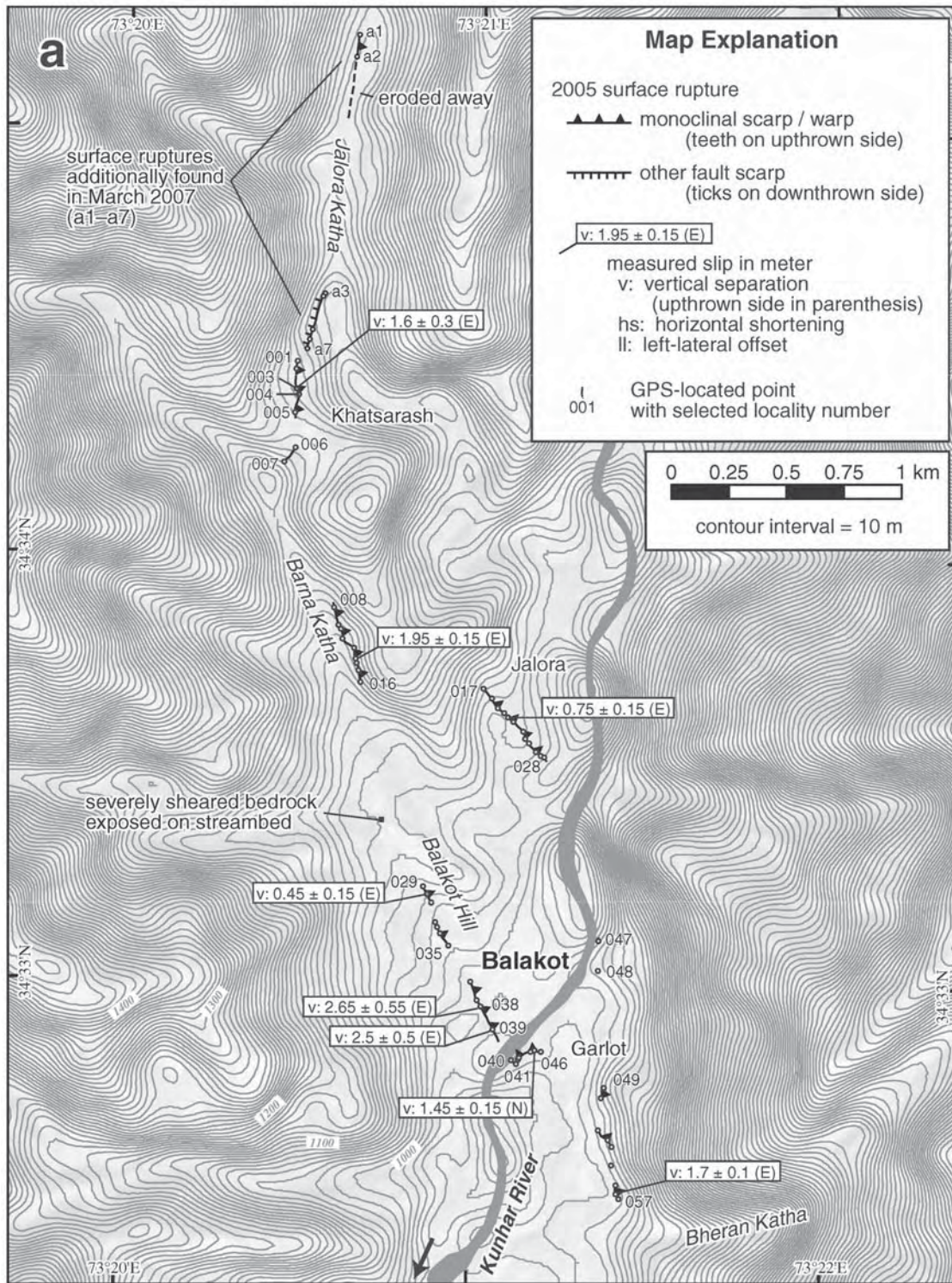


Figure A1. The maps shown in Figure A1 are detailed maps of the surface rupture associated with the 2005 Kashmir earthquake. The index map is shown in Figure 3. Note that some maps (Fig. A1b,c,j) are smaller scale. The location and trace of the surface rupture is determined by a handheld GPS receiver, and GPS-located points are shown by blue dots. Selected locality numbers are indicated by three-digit numbers increasing to southeast. Measured slip across the surface rupture is also shown with the up-thrown side direction in parentheses. Topographic contour lines are produced by the ASTER-based digital elevation model. The map explanation is in Fig. A1a. (a) Locations 001–057; (b) and (c) locations 058–114; (d) locations 115–149; (e) locations 150–187; (f) locations 188–271; (g) locations 272–343; (h) locations 344–369; (i) locations 370–459; (j) locations 460–490. (Continued)

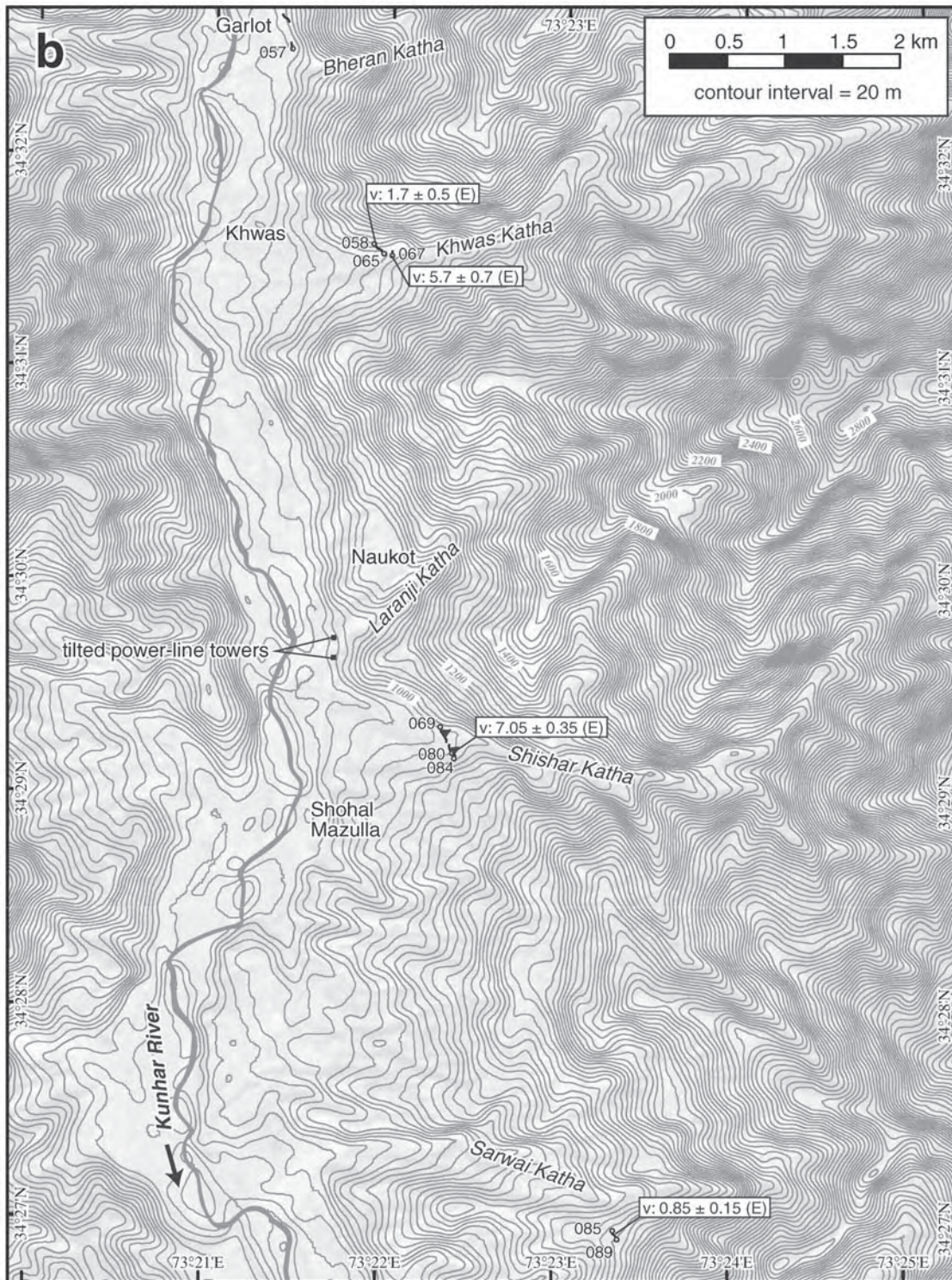


Figure A1. Continued.

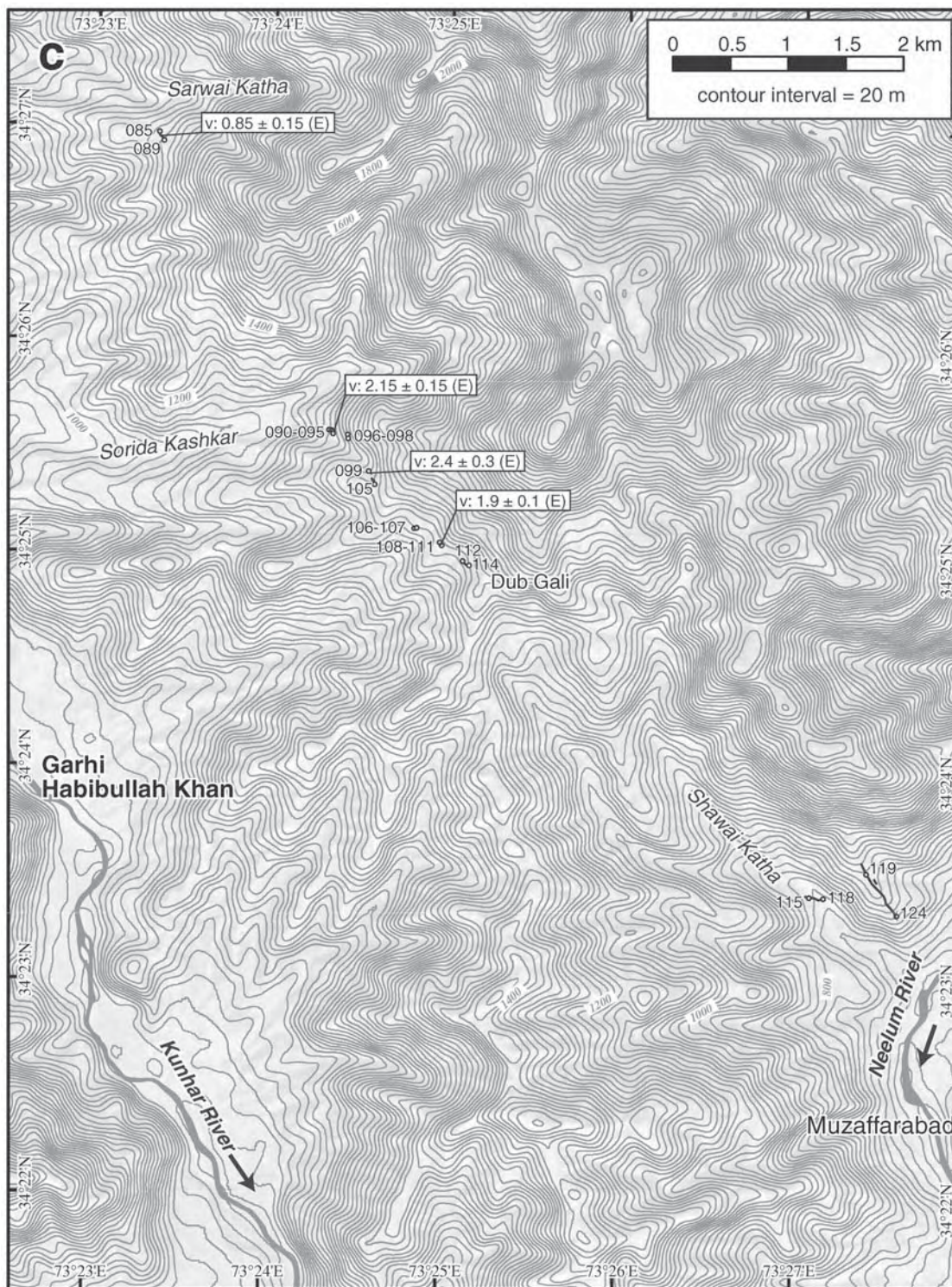


Figure A1. Continued.

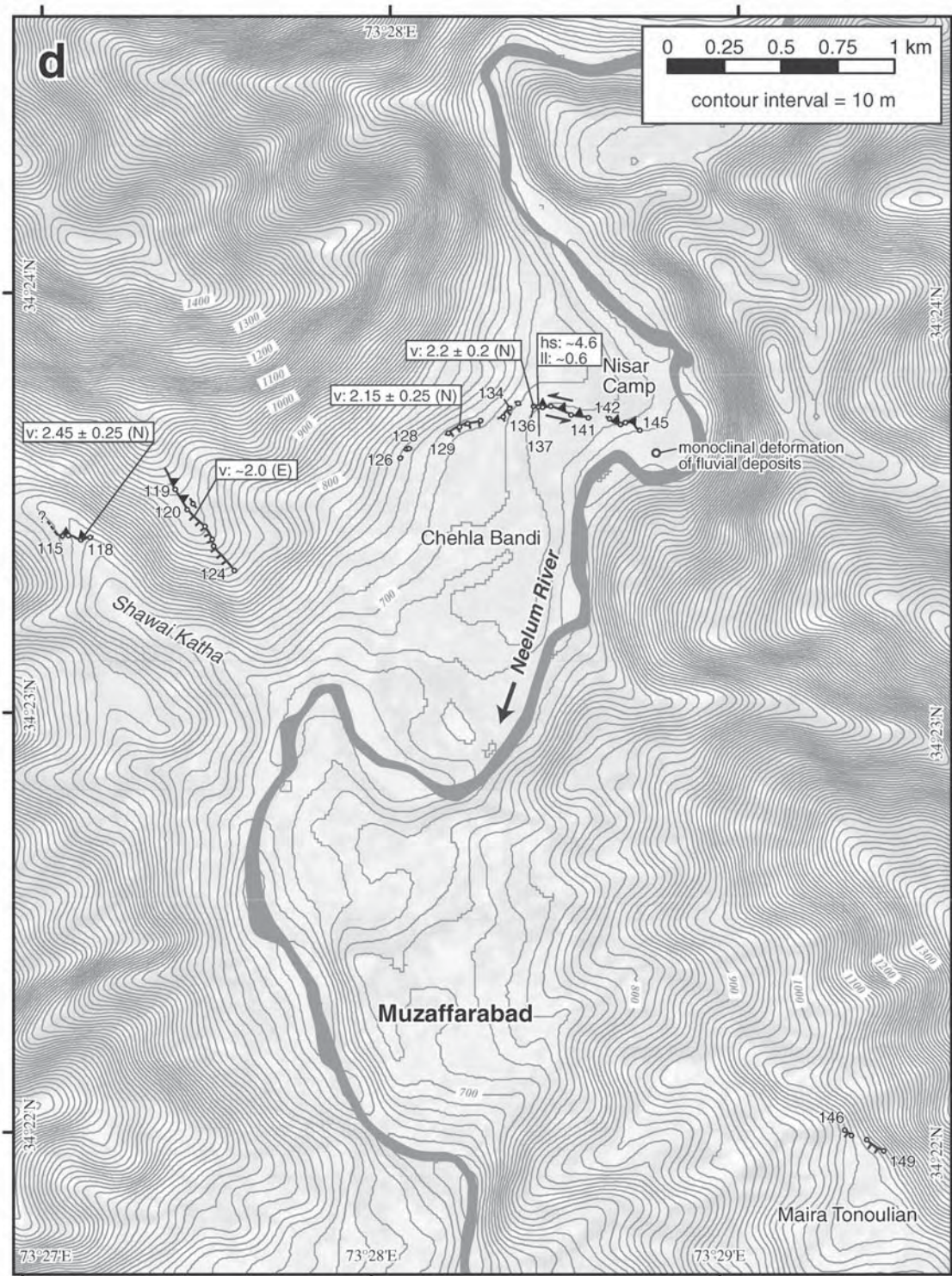


Figure A1. Continued.

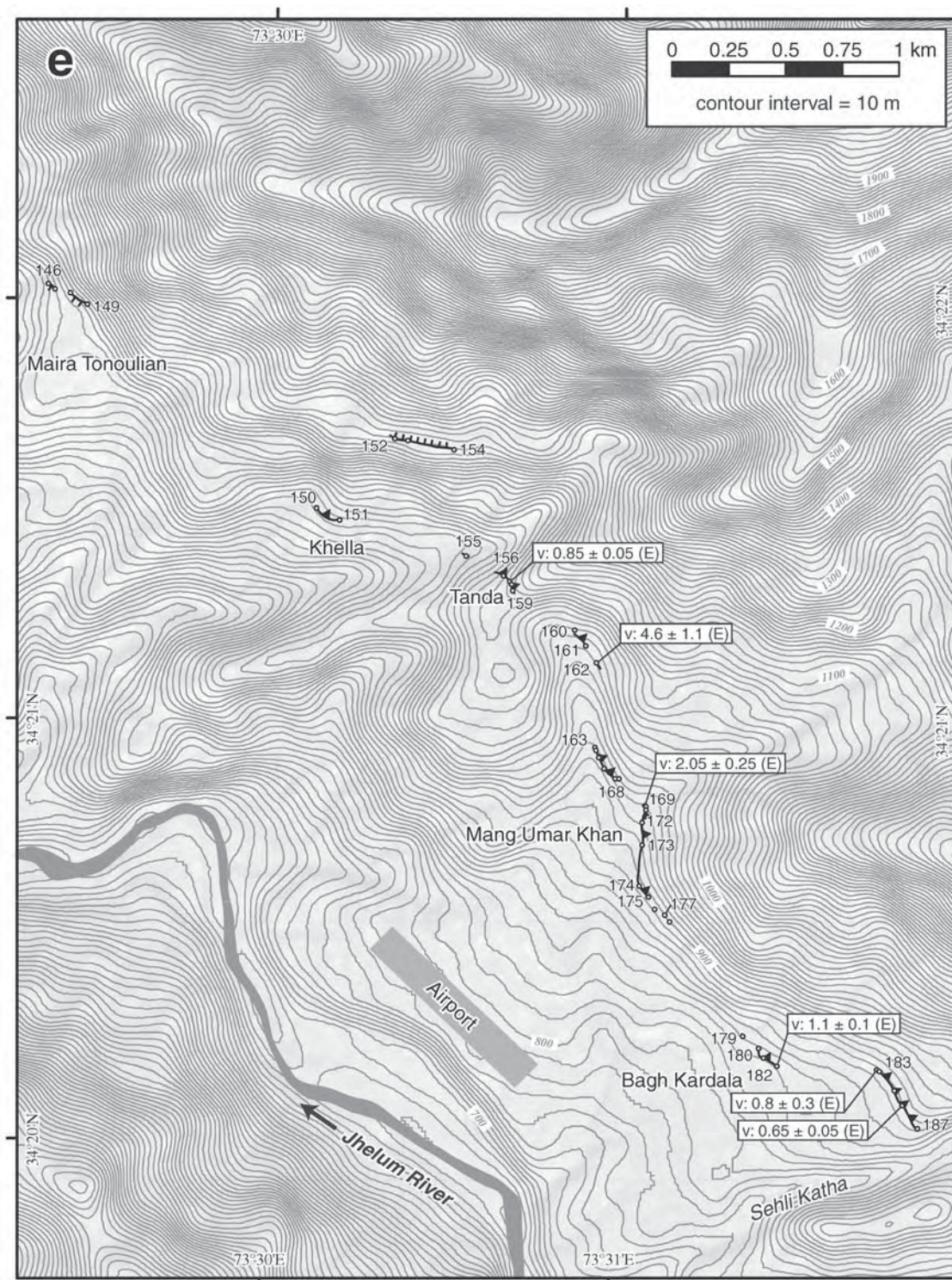


Figure A1. Continued.

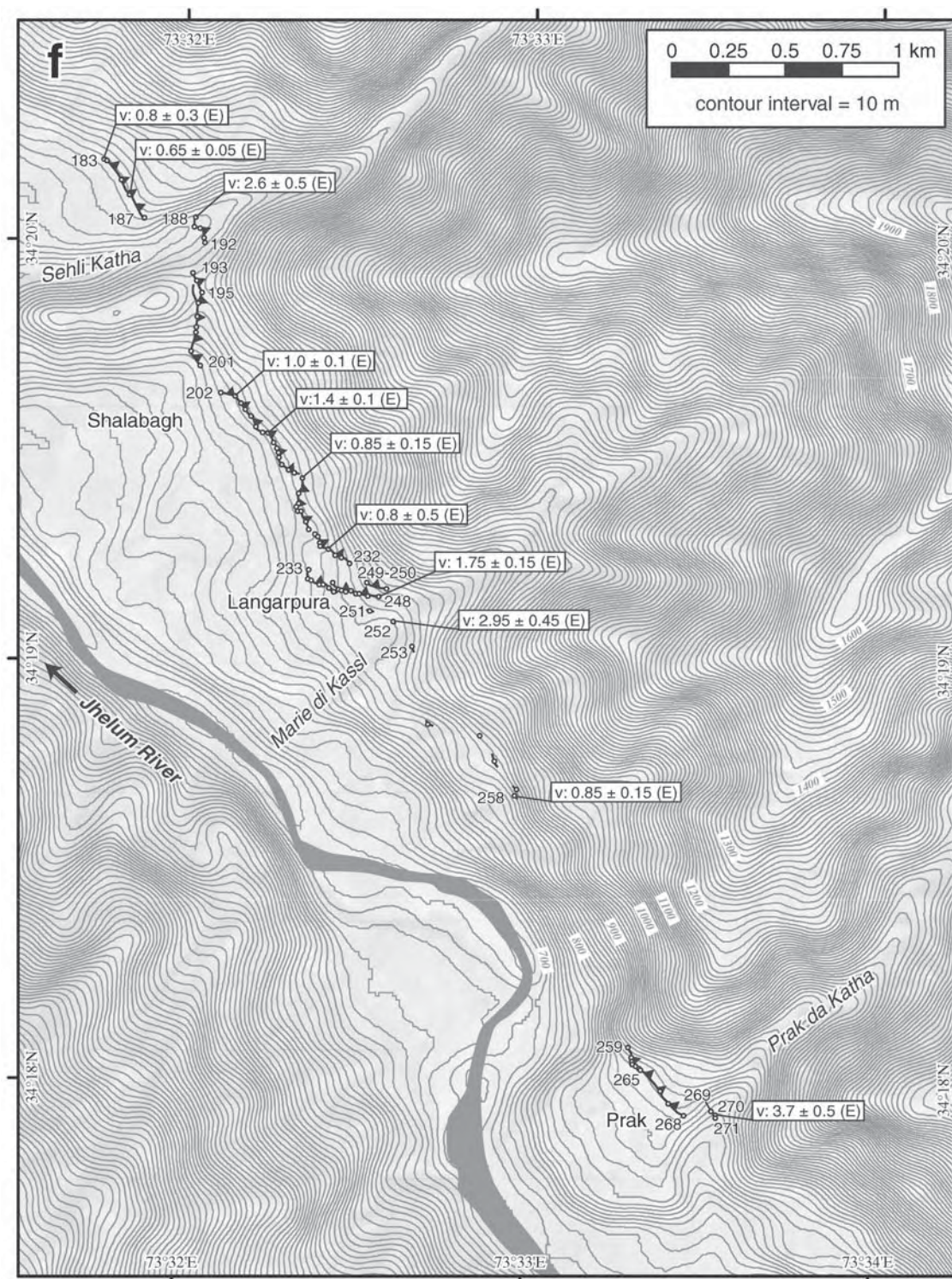


Figure A1. Continued.

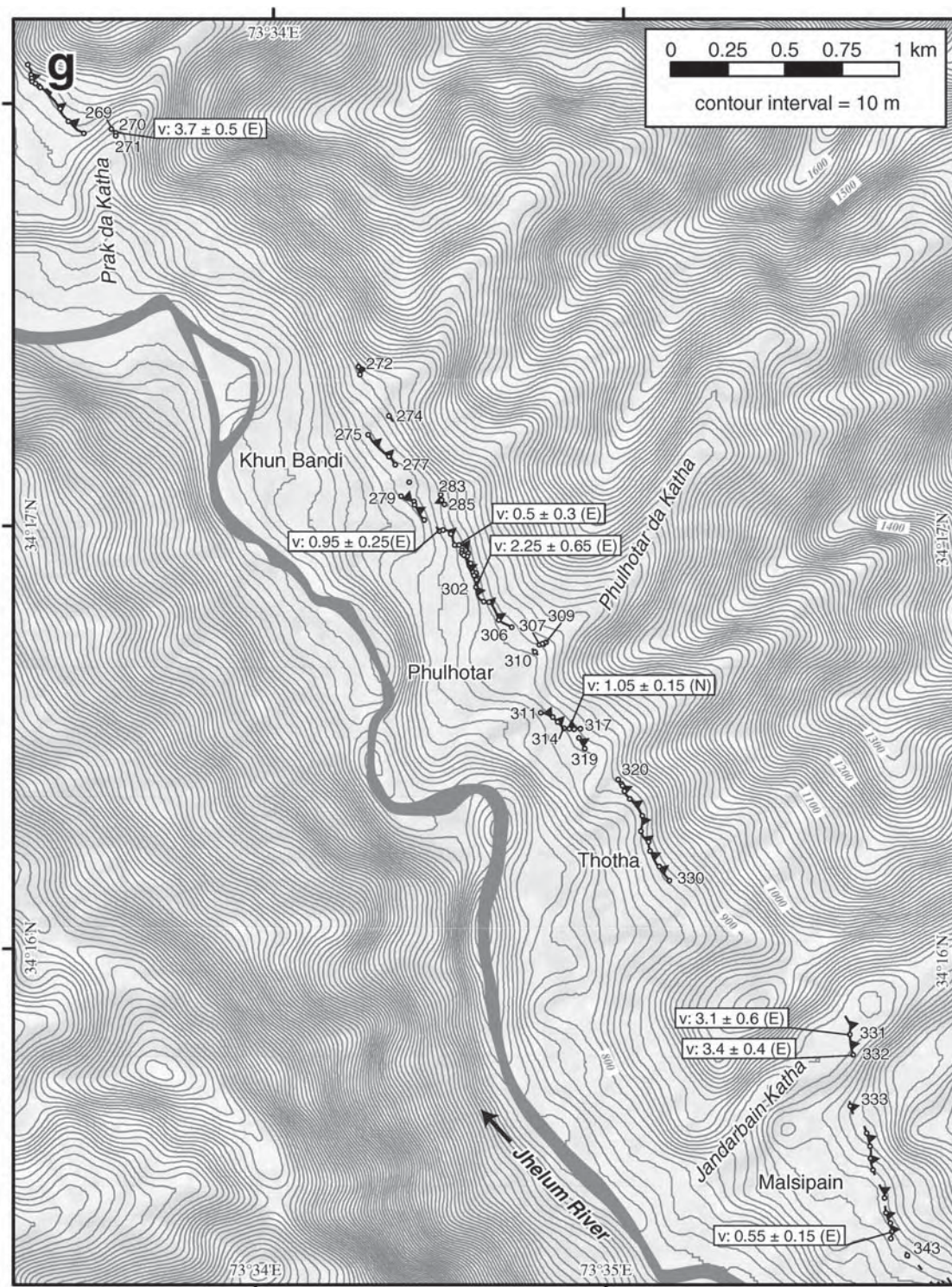


Figure A1. Continued.

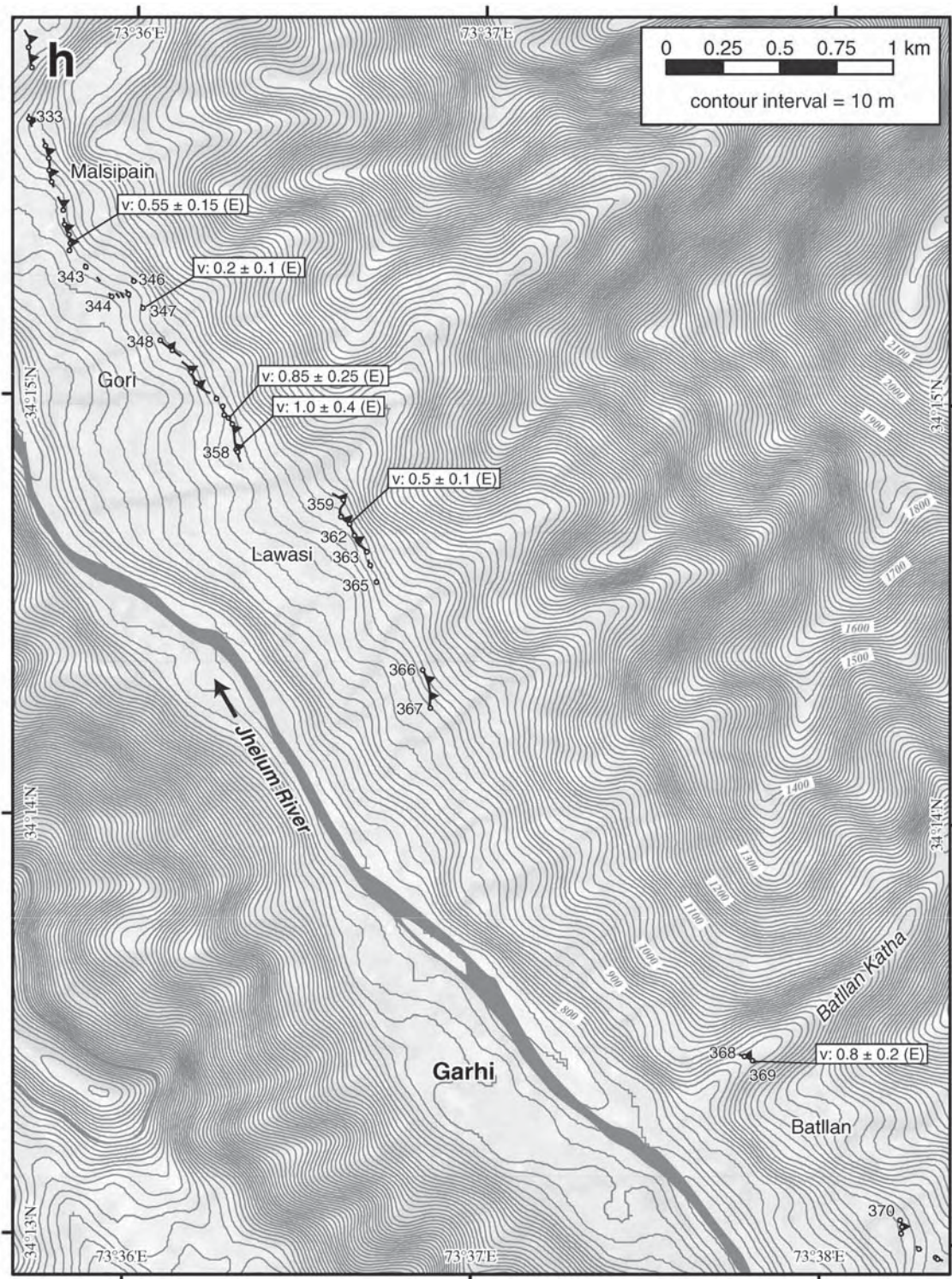


Figure A1. Continued.

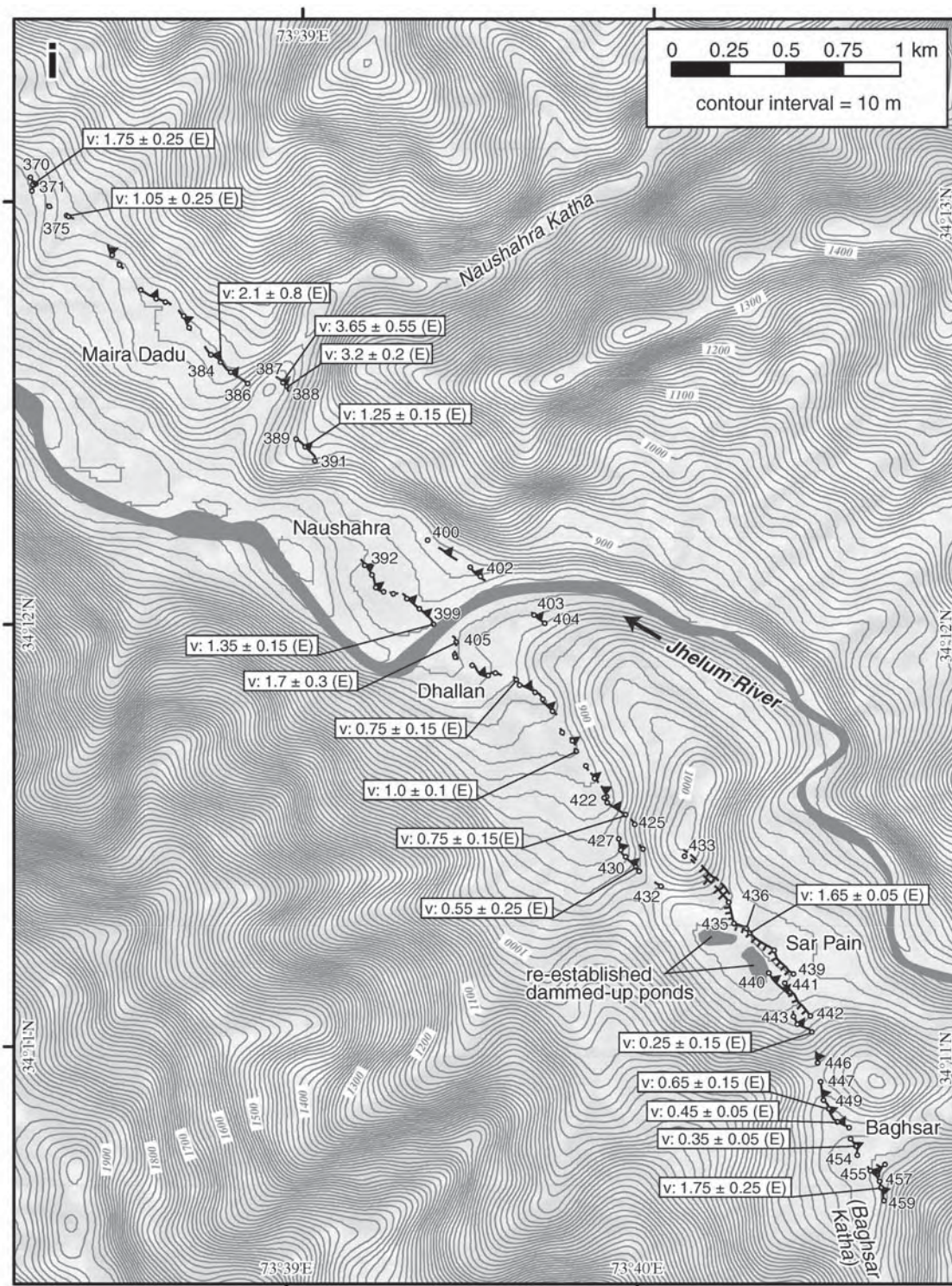


Figure A1. Continued.

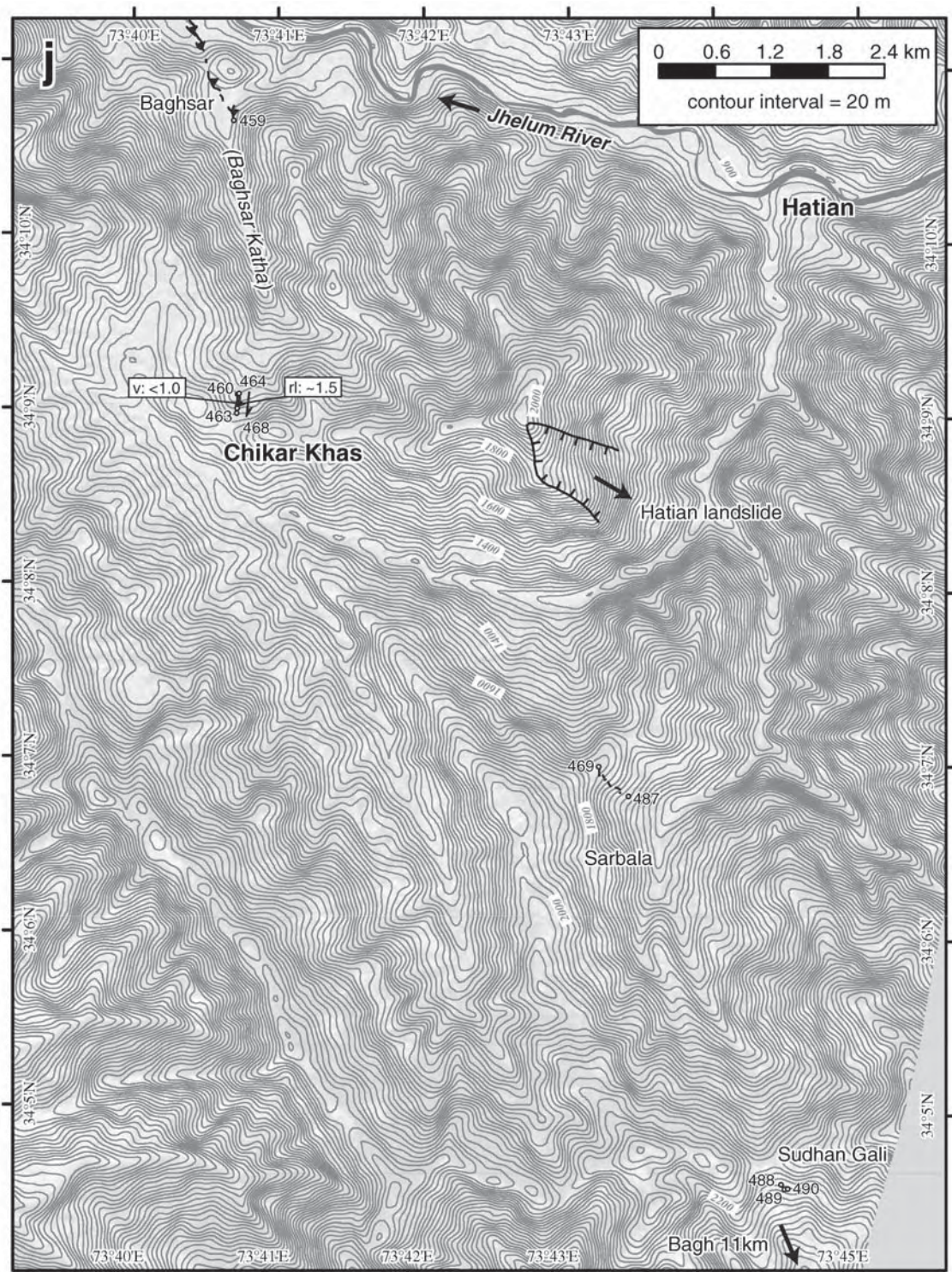


Figure A1. Continued.

Geological Survey of Japan
National Institute of Advanced Industrial Science and Technology
Central 7, 1-1-1 Higashi
Tsukuba 305-8567, Japan
(H.K., H.K., Y.A.)

Faculty of Environmental Studies
Hiroshima Institute of Technology
2-1-1 Miyake, Saeki-ku
Hiroshima, 731-5193, Japan
(T.N.)

Department of Geophysics
Kyoto University
Kitashirakawa-oiwake-cho, Sakyo-ku
Kyoto 606-8502, Japan
(H.T.)

Research Center for Seismology, Volcanology, and Disaster Mitigation
Nagoya University
Furo-cho, Chikusa-ku
Nagoya 464-8601, Japan
(N.S.)

Geological Survey of Pakistan, Islamabad
Plot No. 84, H-8/1
Islamabad, Pakistan
(S.S.A., A.M., A.A.A., A.B.K.)

Geological Survey of Pakistan, Peshawar
Plot No. 10 & 11, Sector B-1, Phase-5
Hayatabad, Peshawar, Pakistan
(W.K., A.H., M.A.)

Department of Geosciences
Oregon State University
104 Wilkinson Hall
Corvallis, Oregon 97331
(R.S.Y.)

Center for Neotectonic Studies
University of Nevada, Reno
1664 North Virginia
Reno, Nevada 89557
(S.G.W.)

Manuscript received 20 March 2007